Exploring neutrino oscillations with superbeams

V. Barger

Department of Physics, University of Wisconsin, Madison, Wisconsin 53706

S. Geer and R. Raja

Fermi National Accelerator Laboratory, P.O. Box 500, Batavia, Illinois 60510

K. Whisnant

Department of Physics and Astronomy, Iowa State University, Ames, Iowa 50011
(Received 4 December 2000; published 2 May 2001)

We consider the medium- and long-baseline oscillation physics capabilities of intense muon-neutrino and muon-antineutrino beams produced using future upgraded megawatt-scale high-energy proton beams. In particular we consider the potential of these conventional neutrino ''superbeams'' for observing $\nu_\mu \rightarrow \nu_e$ oscillations, determining the hierarchy of neutrino mass eigenstates, and measuring CP violation in the lepton sector. The physics capabilities of superbeams are explored as a function of the beam energy, baseline, and the detector parameters (fiducial mass, background rates, and systematic uncertainties on the backgrounds). The trade-offs between very large detectors with poor background rejection and smaller detectors with excellent background rejection are illustrated. We find that, with an aggressive set of detector parameters, it may be possible to observe $\nu_\mu \rightarrow \nu_e$ oscillations with a superbeam provided that the amplitude parameter $\sin^2 2\theta_{13}$ is larger than a few $\times 10^{-3}$. If $\sin^2 2\theta_{13}$ is of order 10^{-2} or larger, then the neutrino mass hierarchy can be determined in long-baseline experiments, and if in addition the large mixing angle MSW solution describes the solar neutrino deficit, then there is a small region of parameter space within which maximal CP violation in the lepton sector would be observable (with a significance of a few standard deviations) in a low-energy medium-baseline experiment. We illustrate our results by explicitly considering massive water Cherenkov and liquid argon detectors at superbeams with neutrino energies ranging from 1 GeV to 15 GeV, and baselines ranging from 295 km to 9300 km. Finally, we compare the oscillation physics prospects at superbeams with the corresponding prospects at neutrino factories. The sensitivity at a neutrino factory to CP violation and the neutrino mass hierarchy extends to values of the amplitude parameter $\sin^2 2\theta_{13}$ that are one to two orders of magnitude lower than at a superbeam.

I. INTRODUCTION

Measurements [1,2] of the neutrino flux produced by cosmic ray interactions in the atmosphere [3] have led to a major breakthrough in our understanding of the fundamental properties of neutrinos. The early observations of the atmospheric neutrino interaction rates found a muon-to-electron event ratio of about 0.6 times the expected ratio. This μ/e anomaly was interpreted [4] as evidence for neutrino oscillations with a large amplitude and neutrino mass-squared difference $\delta m^2_{atm} \sim 10^{-2}$ eV^2. Continued experimental studies [1,2], especially by the SuperKamiokande (SuperK) Collaboration, have firmly established that the deviation of the μ/e ratio from expectation is due to a deficit of muon events. This muon deficit increases with zenith angle, and hence with path length, and is consistent with expectations for muon-neutrino oscillations to some other neutrino flavor or flavors ($\nu_\mu \rightarrow \nu_x$) with maximal or near-maximal amplitude and $\delta m^2_{atm} \simeq 3.5 \times 10^{-3}$ eV^2. In principle ν_x could be ν_e (electron-neutrino), ν_τ (tau-neutrino), or ν_s (sterile neutrino) [5]. However, the observed ν_e flux is in approximate agreement with the predicted ν_e flux for all zenith angles [1], which rules out $\nu_\mu \rightarrow \nu_e$ oscillations with large amplitude. The null results from the CHOOZ and Palo Verde reactor $\bar{\nu}_e$ disappearance experiments [6] also exclude $\bar{\nu}_e \rightarrow \bar{\nu}_\mu$ oscilla-

tions at a mass-squared-difference scale $> 10^{-3}$ eV^2 with amplitude > 0.1. Furthermore, large amplitude $\nu_\mu \rightarrow \nu_s$ oscillations at the δm^2_{atm} scale are also excluded by SuperK. This is because $\nu_\mu \rightarrow \nu_s$ oscillations are expected to be significantly affected by propagation through matter [7,8], causing a distortion in the zenith-angle distribution at large angles (corresponding to long path lengths) that is not present in the data [9]. The zenith-angle distribution observed by SuperK excludes $\nu_\mu \rightarrow \nu_s$ oscillations of maximal amplitude at 99% confidence level [9]. We conclude that, if the oscillation interpretation of the atmospheric neutrino deficit is correct, the dominant mode must be $\nu_\mu \rightarrow \nu_\tau$ oscillation, with the possibility of some smaller amplitude muon-neutrino oscillations to sterile and/or electron-neutrinos [10].

An exotic alternative interpretation [11] of the atmospheric neutrino disappearance results is that a neutrino mass eigenstate, which is a dominant component of the ν_μ state, decays to a lighter mass-eigenstate and a Majoron [12]. The first oscillation minimum in $\nu_\mu \rightarrow \nu_\mu$ must be observed or excluded to differentiate neutrino oscillations from neutrino decays. Unfortunately, the SuperK neutrino-energy and angular-resolution functions smear out the characteristic ν_μ event rate dip that would correspond to the first oscillation minimum, which cannot therefore be resolved.

Progress in establishing neutrino oscillations at the atmo-

63 113011-1

spheric scale is expected in the near future at accelerator neutrino sources with detectors at medium to long baselines. The K2K experiment, from KEK to SuperK [13], with a baseline $L = 250$ km and average neutrino energy $\langle E_\nu \rangle = 1.4$ GeV, is underway. Their preliminary results are in excellent agreement with the oscillation expectations (27 events are observed, whereas 27 events would be expected with oscillations and 40 events for no oscillations [13]). The MINOS experiment from Fermilab to Soudan [14] with $L = 730$ km and $\langle E_\nu \rangle = 3.5$ GeV, which begins operation in 2003, is expected to resolve the first oscillation minimum in $\nu_\mu \leftrightarrow \nu_\mu$ and to search for $\nu_\mu \leftrightarrow \nu_e$ oscillations at the δm^2_{atm} scale with an amplitude sensitivity of 10^{-2}. Beginning in 2005, similar physics measurements will be made by the ICARUS [15] and OPERA [16] experiments with neutrinos of average energy $\langle E_\nu \rangle \simeq 20$ GeV from CERN detected at $L \simeq 730$ km in the Gran Sasso laboratory.

In addition to the atmospheric neutrino deficit, there are other possible indications of neutrino oscillations. In particular, the long-standing deficit of solar neutrinos [17–20] compared to the standard solar model (SSM) predictions [21] is widely interpreted as an oscillation depletion of the ν_e flux. Note that helioseismology and other solar observations stringently limit uncertainties in the central temperature of the sun and other solar model parameters [22]. The ν_e deficit relative to prediction is about one-half for the water Cherenkov [18,19] and gallium experiments [20], with the chlorine experiment [17] finding a suppression of about one-third. The latest solar neutrino results from SuperK show an electron recoil spectrum that is flat in energy, and exhibits no significant day-night or seasonal variation [23].

An industry has developed to extract the allowed ranges of $\delta m^2_{\text{solar}}$ and ν_e mixing angles that can account for the solar neutrino data. The analyses take account of the coherent scattering of ν_e on matter [7], both in the Sun (the MSW effect [24]) and in the Earth [25]. These matter effects can make significant modifications to vacuum oscillation amplitudes. Until recently, four viable regions of the parameter space were found in global fits to the data:

(i) LMA—large mixing angle with small matter effects ($\delta m^2_{\text{solar}} \approx 10^{-5}$–$10^{-4}$ eV^2),

(ii) SMA—small mixing angle with large matter effects ($\delta m^2_{\text{solar}} \approx 10^{-5}$ eV^2),

(iii) LOW—large-angle mixing with quasi-vacuum amplitude ($\delta m^2_{\text{solar}} \approx 10^{-7}$ eV^2),

(iv) VO—large-angle vacuum mixing with small matter effects ($\delta m^2_{\text{solar}} \approx 10^{-10}$ eV^2).

The latest global solar neutrino analysis by the SuperK Collaboration [23] strongly favors solar ν_e oscillations to active neutrinos (ν_μ and/or ν_τ) in the LMA region. A very small area in the LOW region is also allowed at 99% C.L., while the SMA and VO regions are rejected at 99% C.L. However, other global analyses disagree that the latter regions are excluded [26]. Moreover, $\nu_e \rightarrow \nu_s$ solar oscillations may also still be viable [27,28]. The relative weighting of different experiments (e.g. inclusion or exclusion of the Cl data) and whether the ^{8}B flux is held fixed at its SSM value or allowed to float in the global fits presumably account in part for the differences in conclusions. It is expected that the KamLAND reactor experiment [29] will be able to measure $|\delta m^2_{21}|$ to $\pm 10\%$ accuracy and $\sin^2 2\theta_{12}$ to ± 0.1 accuracy [30] if the LMA solar solution is correct.

Finally, the Liquid Scintillation Neutrino Detector (LSND) accelerator experiment [31] reports evidence for possible $\bar\nu_\mu \rightarrow \bar\nu_e$ and $\nu_\mu \rightarrow \nu_e$ oscillations with very small amplitude and $\delta m^2_{\text{LSND}} \approx 1$ eV^2. If, in addition to the LSND observations, the atmospheric and solar effects are also to be explained by oscillations, then three distinct δm^2 scales are needed, requiring a sterile neutrino in addition to the three active neutrino flavors [5,10,27,28]. The MiniBooNE experiment at Fermilab [32] is designed to cover the full region of oscillation parameters indicated by LSND.

The principal goals of our analyses are to examine the relative merits of different neutrino ''superbeam'' scenarios, where we define a neutrino superbeam as a conventional neutrino beam generated by $\pi^\pm$ decays, but using a very intense megawatt- (MW-) scale proton source. In particular, we are interested in the physics reach in medium- and long-baseline experiments with a neutrino superbeam, and how this reach depends upon the beam energy, baseline, and the parameters of the neutrino detector. As representative examples we explicitly consider water Cherenkov, liquid argon and iron scintillator detectors. However, we note that there is room for new detector ideas, detector optimization, and possibly an associated detector research and development program. Therefore, results are presented that apply to any detector for which the effective fiducial mass and background rates can be specified. Finally, we will discuss the role that neutrino superbeams might play [33,34] en route to a neutrino factory [35,36]. Our calculations are performed within a three-neutrino oscillation framework with the parameters chosen to describe the atmospheric neutrino deficit and the solar neutrino deficit assuming the LMA solution. However, our considerations for long-baseline experiments are relevant even if there are additional short-baseline oscillation effects associated with a fourth neutrino [37].

The central objective of long-baseline neutrino oscillation experiments is to determine the parameters of the neutrino mixing matrix and the magnitudes and signs of the neutrino mass-squared differences; the signs fix the hierarchy of the neutrino mass eigenstates [38]. For three neutrinos (ν_e, ν_μ, ν_τ) the mixing matrix relevant to oscillation phenomena can be specified by three angles ($\theta_{23}, \theta_{12}, \theta_{13}$) and a phase δ associated with CP violation [see Eq. (9) below]. There are only two independent mass-squared differences (e.g. δm^2_{32} and δm^2_{21}) for three neutrinos. The muon-disappearance measurements at SuperK constrain $\theta_{23} \sim \pi/2$ and $\delta m^2_{32} \sim 3 \times 10^{-3}$ eV^2. The other parameter that enters at the leading δm^2_{32} oscillation scale is θ_{13}, and its measurement requires the observation of neutrino appearance in $\nu_e \rightarrow \nu_\mu$, $\nu_\mu \rightarrow \nu_e$, or $\nu_e \rightarrow \nu_\tau$ oscillations.

In long-baseline experiments, if θ_{13} is nonzero, matter effects [7,39,40] modify the probability for oscillations involving a ν_e or $\bar\nu_e$ in a way that can be used to determine the sign of δm^2_{32} [38,41–43]. Matter effects give apparent CP violation, but this may be disentangled from intrinsic

CP-violation effects [38,44–52] at optimally chosen baselines. Matter can also modify the effects of intrinsic *CP* or *T* violation [53]. Intrinsic *CP* violation may also be studied at short baselines where matter effects are relatively small [54,55]. *CP*-violating effects enter only for values of L/E_ν where oscillations associated with the subleading δm_{21}^2 become significant [56,57]. The most challenging goal of accelerator-based neutrino oscillation experiments is to detect, or place stringent limits on, *CP* violation in the lepton sector. We will address the extent to which this may be possible with conventional superbeams.

II. THREE-NEUTRINO FORMALISM

The flavor eigenstates ν_α ($\alpha = e, \mu, \tau$) are related to the mass eigenstates ν_j ($j = 1, 2, 3$) in vacuum by

$$\nu_\alpha = \sum_j U_{\alpha j} \nu_j, \tag{1}$$

where U is a unitary 3×3 mixing matrix. The propagation of neutrinos through matter is described by the evolution equation [7,58]

$$i \frac{d\nu_\alpha}{dx} = \sum_\beta \left(\sum_j U_{\alpha j} U_{\beta j}^* \frac{m_j^2}{2E_\nu} + \frac{A}{2E_\nu} \delta_{\alpha e} \delta_{\beta e} \right) \nu_\beta, \tag{2}$$

where $x = ct$ and $A/2E_\nu$ is the amplitude for coherent forward charged-current ν_e scattering on electrons,

$$A = 2\sqrt{2} \, G_F Y_e \rho E_\nu$$
$$= 1.52 \times 10^{-4} \ \text{eV}^2 \times Y_e \rho \, (\text{g/cm}^3) \times E_\nu \, (\text{GeV}), \tag{3}$$

where $Y_e(x)$ is the electron fraction and $\rho(x)$ is the matter density. In the Earth's crust the average density is typically 3–4 gm/cm^3 and $Y_e \simeq 0.5$. The propagation equations can be re-expressed in terms of mass-squared differences:

$$i \frac{d\nu_\alpha}{dx} = \sum_\beta \frac{1}{2E_\nu} (\delta m_{31}^2 U_{\alpha 3} U_{\beta 3}^* + \delta m_{21}^2 U_{\alpha 2} U_{\beta 2}^* + A \delta_{\alpha e} \delta_{\beta e}), \tag{4}$$

where $\delta m_{jk}^2 = m_j^2 - m_k^2$. We assume $|\delta m_{21}^2| \ll |\delta m_{32}^2|$, and that the sign of δm_{32}^2 can be either positive or negative, corresponding to the case where the most widely separated mass eignstate is either above or below, respectively, the other two mass eigenstates. Thus the sign of δm_{32}^2 determines the ordering of the neutrino masses. The evolution equations can be solved numerically taking into account the dependence of the density on depth using the density profile from the preliminary reference earth model [59]. We integrate the equations numerically along the neutrino path using a Runge-Kutta method. The step size at each point along the path is taken to be 1% of the shortest oscillation wavelength given by the two scales δm_{32}^2 and A.

It is instructive to examine analytic expressions for the vacuum probabilities. We introduce the notation

$$\Delta_{jk} \equiv \delta m_{jk}^2 L / 4E_\nu = 1.27 (\delta m_{jk}^2 / \text{eV}^2)(L/\text{km})(\text{GeV}/E_\nu). \tag{5}$$

The vacuum probabilities are then given by

$$\begin{aligned} P(\nu_\alpha \to \nu_\beta) = &-4 \, \text{Re}(U_{\alpha 2} U_{\alpha 3}^* U_{\beta 2}^* U_{\beta 3}) \sin^2 \Delta_{32} \\ &-4 \, \text{Re}(U_{\alpha 1} U_{\alpha 3}^* U_{\beta 1}^* U_{\beta 3}) \sin^2 \Delta_{31} \\ &-4 \, \text{Re}(U_{\alpha 1} U_{\alpha 2}^* U_{\beta 1}^* U_{\beta 2}) \sin^2 \Delta_{21} \pm 2JS, \end{aligned} \tag{6}$$

where J is the *CP*-violating invariant [60,61],

$$J = \text{Im}(U_{e2} U_{e3}^* U_{\mu 2}^* U_{\mu 3}), \tag{7}$$

and S is the associated dependence on L and E_ν,

$$S = \sin 2\Delta_{21} + \sin 2\Delta_{32} - \sin 2\Delta_{31}. \tag{8}$$

The mixing matrix can be specified by 3 mixing angles $(\theta_{32}, \theta_{12}, \theta_{13})$ and a *CP*-violating phase (δ). We adopt the parametrization

$$U = \begin{pmatrix} c_{13}c_{12} & c_{13}s_{12} & s_{13}e^{-i\delta} \\ -c_{23}s_{12} - s_{13}s_{23}c_{12}e^{i\delta} & c_{23}c_{12} - s_{13}s_{23}s_{12}e^{i\delta} & c_{13}s_{23} \\ s_{23}s_{12} - s_{13}c_{23}c_{12}e^{i\delta} & -s_{23}c_{12} - s_{13}c_{23}s_{12}e^{i\delta} & c_{13}c_{23} \end{pmatrix}, \tag{9}$$

where $c_{jk} \equiv \cos \theta_{jk}$ and $s_{jk} \equiv \sin \theta_{jk}$. We can restrict the angles to the first quadrant, $0 \leq \theta_{ij} \leq \pi/4$, with δ in the range $-\pi \leq \delta \leq \pi$. In this parametrization J is given by

$$J = s_{13}c_{13}^2 s_{12}c_{12}s_{23}c_{23}s_\delta = \frac{1}{8}\sin 2\theta_{23}\sin 2\theta_{12}\sin 2\theta_{13}c_{13}s_\delta. \tag{10}$$

For convenience we also define

$$K = s_{13}c_{13}^2 s_{12}c_{12}s_{23}c_{23}c_\delta = \frac{1}{8}\sin 2\theta_{23}\sin 2\theta_{12}\sin 2\theta_{13}c_{13}c_\delta. \tag{11}$$

Then the vacuum appearance probabilities are given by

$$P(\nu_\mu \to \nu_e) = [s_{23}^2 s_{12}^2 \sin^2 2\theta_{13} - 4K]\sin^2 \Delta_{32} + [s_{23}^2 c_{12}^2 \sin^2 2\theta_{13} + 4K]\sin^2 \Delta_{31}$$
$$+ [c_{13}^2(c_{23}^2 - s_{13}^2 s_{23}^2)\sin^2 2\theta_{12} + 4K\cos 2\theta_{12}]\sin^2 \Delta_{21} + 2JS, \tag{12}$$

$$P(\nu_\mu \to \nu_\tau) = [c_{13}^2(c_{12}^2 - s_{12}^2 s_{13}^2)\sin^2 2\theta_{23} + 4K\cos \theta_{23}]\sin^2 \Delta_{32}$$
$$+ [c_{13}^2(s_{12}^2 - c_{12}^2 s_{13}^2)\sin^2 2\theta_{23} - 4K\cos \theta_{23}]\sin^2 \Delta_{31}$$
$$+ 2[\sin^2 2\theta_{23}(s_{13}^2 - s_{12}^2 c_{12}^2(1 + s_{13}^2)^2) + s_{13}^2 \sin^2 2\theta_{12}(1 + \sin^2 2\theta_{23} s_\delta^2)$$
$$+ \sin 2\theta_{12}\cos\theta_{12}\sin 2\theta_{23}\cos\theta_{23}s_{13}c_\delta(1 + s_{13}^2)]\sin^2 \Delta_{21} - 2JS, \tag{13}$$

$$P(\nu_e \to \nu_\tau) = [c_{23}^2 s_{12}^2 \sin^2 2\theta_{13} + 4K]\sin^2 \Delta_{32} + [c_{23}^2 c_{12}^2 \sin^2 2\theta_{13} - 4K]\sin^2 \Delta_{31}$$
$$+ [c_{13}^2(s_{23}^2 - s_{13}^2 c_{23}^2)\sin^2 2\theta_{12} - 4K\cos 2\theta_{12}]\sin^2 \Delta_{21} + 2JS. \tag{14}$$

The corresponding probabilities $P(\bar\nu_\alpha \to \bar\nu_\beta)$ can be obtained by reversing the sign of δ in the above formulas (only the JS term changes sign in each case). The probabilities for $\bar\nu_\beta \to \bar\nu_\alpha$ are the same as those for $\nu_\alpha \to \nu_\beta$, assuming CPT invariance. Tests of CPT non-invariance are important [62–64] but beyond the scope of the present analysis. The Δ_{ij} are not independent, and can be expressed in terms of $\Delta_{atm} \equiv \Delta_{32}$ and $\Delta_{sun} \equiv \Delta_{21}$. Then $\Delta_{31} = \Delta_{atm} + \Delta_{sun}$ and

$$\sin^2 \Delta_{31} = \sin^2 \Delta_{atm} + \sin^2 \Delta_{sun}\cos 2\Delta_{atm}$$
$$+ \frac{1}{2}\sin 2\Delta_{sun}\sin 2\Delta_{atm}, \tag{15}$$

$$S = 2(\sin 2\Delta_{sun}\sin^2 \Delta_{atm}$$
$$+ \sin 2\Delta_{atm}\sin^2 \Delta_{sun}). \tag{16}$$

Since Eqs. (12)–(16) in their exact form are somewhat impenetrable, we make a few simplifying assumptions to illustrate their typical consequences. First, it is advantageous in long-baseline experiments to operate at an L/E_ν value such that the leading oscillation is nearly maximal, i.e. $\Delta_{atm} \simeq \pi/2$. Since $\delta m_{sun}^2 \ll \delta m_{atm}^2$, $\Delta_{sun} \ll 1$ and to a good approximation we can ignore terms involving $\sin^2 \Delta_{sun}$. Also, since θ_{13} is already constrained by experiment to be small, for the terms involving Δ_{sun} we retain only the leading terms in θ_{13}. Second, at the value $\Delta_{atm} \simeq \pi/2$ for which the leading oscillation is best measured, $\sin 2\Delta_{atm} \simeq 0$. Even if Δ_{atm} is not close to $\pi/2$ for all neutrino energies in the beam, an averaging over the energy spectrum will suppress $\sin 2\Delta_{atm}$ if the neutrinos at the middle of the spectrum have $\Delta_{atm} \simeq \pi/2$. With the above approximations the vacuum oscillation probabilities simplify to

$$P(\nu_\mu \to \nu_e) \simeq \sin^2 \Delta_{atm}(s_{23}^2 \sin^2 2\theta_{13} + 4J\sin 2\Delta_{sun}), \tag{17}$$

$$P(\nu_\mu \to \nu_\tau) \simeq \sin^2 \Delta_{atm}(\sin^2 2\theta_{23} - 4J\sin 2\Delta_{sun}), \tag{18}$$

$$P(\nu_e \to \nu_\tau) \simeq \sin^2 \Delta_{atm}(c_{23}^2 \sin^2 2\theta_{13} + 4J\sin 2\Delta_{sun}). \tag{19}$$

It is interesting to compare the relative sizes of the leading CP-violating (CPV) and CP-conserving (CPC) terms in the $\nu_\mu \to \nu_e$ oscillation probability:

$$\frac{CPV}{CPC} \simeq \frac{4J\sin 2\Delta_{sun}}{s_{23}^2 \sin^2 2\theta_{13}} \simeq \left(\frac{\sin 2\theta_{12}\sin 2\theta_{23}}{2s_{23}^2}\right)\left(\frac{\Delta_{sun}\sin\delta}{\theta_{13}}\right). \tag{20}$$

For the standard three-neutrino solution to the solar and atmospheric data with large-angle mixing in the solar sector, the first fraction on the right-hand side of Eq. (20) is of order unity, and the relative size of the CPV term is

$$\frac{CPV}{CPC} \sim \frac{\Delta_{sun}\sin\delta}{\theta_{13}}. \tag{21}$$

As an example, with $\delta m_{sun}^2 \simeq 1 \times 10^{-4}$ eV^2 and $L/E_\nu \simeq 300$ km/GeV, $\Delta_{sun} \simeq 0.04$; then with $\delta = \pi/2$ and $\sin^2 2\theta_{13} = 0.1$ (its maximum allowed value), the CPV term is about 25% of the CPC term. Smaller values of δm_{21}^2 or $\sin\delta$ decrease the ratio in Eq. (21); smaller values of θ_{13} increase it.

While smaller values of θ_{13} give a larger relative CPV term, they will also reduce the overall $\nu_\mu \to \nu_e$ event rate since the CPC term is proportional to $\sin^2 2\theta_{13}$. The CPV effect may be hard to measure if the event rate is low (due to insufficient flux or a small detector). Because the number of CPC events is proportional to $\sin^2 2\theta_{13}$, the statistical uncertainty in the CPC event rate is proportional to θ_{13} for small θ_{13} and Gaussian statistics. Since the number of CPV events is also proportional to θ_{13}, the size of the CPV signal relative to the statistical uncertainties does not decrease as θ_{13} becomes smaller. Therefore, *a priori* it does not follow that small θ_{13} automatically makes CPV undetectable [65].

On the other hand, even if the event rate is high enough to overcome the statistical uncertainties on the signal, backgrounds will limit the ability to measure CPV. Background considerations place an effective lower bound on the values of $\sin^2 2\theta_{13}$ for which a CPV search can be made. This can

be quantified by noting that the ratio of the number of CPV events N_{CPV} to the uncertainty due to the background is $N_{CPV}/\sqrt{f_B N_0}$ (assuming Gaussian statistics), where N_0 is the number of events without oscillations and f_B is the background fraction. N_{CPV} can be expressed as the CPV part of the oscillation probability times N_0. Using the expression for the probability in Eq. (17), it follows that a 3σ CPV effect in the $\nu_\mu \to \nu_e$ channel requires

$$\sin^2 2\theta_{13} \gtrsim \frac{9}{\Delta_{sun}^2 \sin^2 \delta} \frac{f_B}{N_0}. \qquad (22)$$

For $\delta = \pi/2$ and $\Delta_{sun} = 0.03$, a typical experiment with $f_B = 0.01$ and $N_0 = 10^4$ can detect CPV for $\sin^2 2\theta_{13} \gtrsim 0.01$. The detailed calculations in Sec. V confirm this approximate result.

The preceding discussion applies only when the corrections due to matter are not large, generally when L is small compared to the Earth's radius. Reference [54] gives approximate expressions for the probabilities when the matter corrections are small but not negligible. However, the most striking matter effects occur when the matter corrections are large and the expansions of Ref. [54] are no longer valid (see, e.g., the plots of oscillation probabilities in matter given in Ref. [66]).

Some of the qualitative properties of neutrino oscillations in matter can be determined by considering only the leading oscillation and assuming a constant density. There is an effective mixing angle in matter defined by

$$\sin^2 2\theta_{13}^m = \frac{\sin^2 2\theta_{13}}{\left(\dfrac{A}{\delta m^2} - \cos 2\theta_{13}\right)^2 + \sin^2 2\theta_{13}}, \qquad (23)$$

where A is given in Eq. (3). The oscillation probabilities in the leading oscillation approximation for constant density are [41,67]

$$P(\nu_\mu \to \nu_e) = s_{23}^2 \sin^2 2\theta_{13}^m \sin^2 \Delta_{32}^m,$$

$$P(\nu_\mu \to \nu_\tau) = \sin^2 2\theta_{23}[(\sin \theta_{13}^m)^2 \sin^2 \Delta_{21}^m$$
$$+ (\cos \theta_{13}^m)^2 \sin^2 \Delta_{31}^m$$
$$- (\sin \theta_{13}^m \cos \theta_{13}^m)^2 \sin^2 \Delta_{32}^m],$$

$$P(\nu_e \to \nu_\tau) = c_{23}^2 \sin^2 2\theta_{13}^m \sin^2 \Delta_{32}^m, \qquad (24)$$

where the oscillation arguments are

$$\Delta_{32}^m = \Delta_{atm} S, \quad \Delta_{31}^m = \Delta_{atm} \frac{1}{2}\left[1 + \frac{A}{\delta m_{atm}^2} + S\right],$$

$$\Delta_{21}^m = \Delta_{atm} \frac{1}{2}\left[1 + \frac{A}{\delta m_{atm}^2} - S\right], \qquad (25)$$

and

$$S \equiv \sqrt{\left(\frac{A}{\delta m_{atm}^2} - \cos 2\theta_{13}\right)^2 + \sin^2 2\theta_{13}}. \qquad (26)$$

The Δ_{21}^m term in $P(\nu_\mu \to \nu_\tau)$ must be retained here because it is not necessarily negligible compared to Δ_{31}^m, due to matter effects. The expressions for antineutrinos may be generated by changing the sign of A.

In Eq. (23) there is a resonant enhancement of $\nu_\mu \to \nu_e$ oscillations when $A \simeq \delta m_{atm}^2 \cos 2\theta_{13}$ ($A \simeq -\delta m_{atm}^2 \cos 2\theta_{13}$ for antineutrinos). This occurs for neutrinos when $\delta m_{atm}^2 > 0$ and for antineutrinos when $\delta m_{atm}^2 < 0$. On resonance, there is a suppression for antineutrinos (neutrinos) when $\delta m_{atm}^2 > 0$ ($\delta m_{atm}^2 < 0$). This enhancement of one channel and suppression of the other then gives a fake CP violation due to matter effects.

In the event that the contribution of the sub-leading oscillation is not negligible, the true CPV effects due to δ also enter, but they may be masked by matter effects. Numerical calculations [42] show that for distances larger than 2000 km matter effects dominate the true CPV for $\sin^2 2\theta_{13} > 0.001$ and vice versa for $\sin^2 2\theta_{13} < 0.001$.

As long as $\sin^2 2\theta_{13}$ is not too small, one approach is to have L large enough so that the dominant CPV effect is from matter and the sign of δm_{atm}^2 is clearly determinable; then the true CPV effect can be extracted by considering deviations from the CP-conserving predictions [42]. With large L, the neutrino energies must be high enough that $\Delta_{atm} \simeq \pi/2$ (e.g., $L \sim 3000$ km requires $E_\nu \sim 10$ GeV). An alternative approach is to have short L where the matter effects are relatively small [54]; this usually requires a smaller E_ν to have Δ_{atm} of order $\pi/2$ (e.g., $L \sim 300$ km and $E_\nu \sim 1$ GeV). We will study both of these possibilities in this paper.

For $\sin^2 2\theta_{13} \lesssim 0.001$, the matter effect is similar in size or smaller than the true CPV effect, and it may not be possible to distinguish between large intrinsic CPV with very small θ_{13} from no intrinsic CPV with a moderate-sized θ_{13}. Even in experiments at short distances (where the matter effect is small) the number of appearance events may be too small relative to the background to have a statistically significant difference between the neutrino and antineutrino oscillation probabilities. The existence of intrinsic CP violation may be very difficult to determine in this case.

III. CONVENTIONAL NEUTRINO BEAMS

Conventional neutrino beams are produced using a pion decay channel. If the pions are charge-sign selected so that only positive (negative) particles are within the channel, the pion decays $\pi^+ \to \mu^+ \nu_\mu$ ($\pi^- \to \mu^- \bar\nu_\mu$) will produce a beam of muon neutrinos (antineutrinos). The beams will also contain small components of ν_e and $\bar\nu_e$ from kaon and muon decays. For a positive beam, the dominant decays that contribute to the ν_e component are $K^+ \to \pi^0 e^+ \nu_e$ and $\mu^+ \to e^+ \nu_e \bar\nu_\mu$. If the pion beam has not been charge-sign selected there will also be a contribution from $K_L^0 \to \pi^\pm e^\mp \nu_e$ decays. The $\nu_e + \bar\nu_e$ ''contamination'' can be minimized using beam optics that disfavor decays occurring close to the

target [note: $\tau(K^{\pm}) \sim 0.5\tau(\pi^{\pm})$], and choosing a short decay channel to reduce the contribution from muon decays. These strategies enhance the flavor purity of the beam, but reduce the beam flux. Depending on the beamline design, the resulting $\nu_e + \bar{\nu}_e$ contamination is typically at the few parts in 100 to a few parts in 1000 level. The intrinsic ν_e component in the beam produces a background that must be subtracted in a $\nu_\mu \to \nu_e$ oscillation search. Ultimately, the systematic uncertainty associated with the background subtraction will degrade the sensitivity of the oscillation measurement.

To maximize the neutrino flux in the forward direction it is desirable that the pion beam divergence is small within the decay channel. The required radial focusing can be provided by a quadrupole channel and/or magnetic horns. The beamline optics (dipoles, horns, and quadrupoles) determine the peak pion energy and energy spread within the decay channel, and hence determine the neutrino spectrum. If the optics are designed to accept a large pion momentum spread the resulting wide band beam (WBB) will contain a large neutrino flux with a broad energy spectrum. If the optics are designed to accept a smaller pion momentum spread, the resulting narrow band beam (NBB) will have a narrower energy spread, but a smaller flux.

Detectors and backgrounds

We are primarily interested in searching for, and measuring, $\nu_\mu \to \nu_e$ and $\bar{\nu}_\mu \to \bar{\nu}_e$ oscillations. The experimental signature for these oscillation modes is the appearance of an energetic electron or positron in a charged-current (CC) event. The electron must be separated from the hadronic remnants produced by the fragmenting nucleon. Backgrounds can arise from (i) energetic neutral pions that are produced in neutral-current (NC) interactions, and subsequently fake a prompt-electron signature, (ii) energetic neutral pions that are produced in CC interactions in which the muon is undetected, and the π^0 fakes an electron, (iii) charm production and semileptonic decay, and (iv) $\nu_\mu \to \nu_\tau$ oscillations followed by decay of the tau-lepton to an electron. Backgrounds (iii) and (iv) can be suppressed using a low-energy neutrino beam.

Background (i) is potentially the most dangerous since leading π^0 production in NC events is not uncommon. Indeed, in a recent study [68,69] using a low energy ν_μ beam it has been shown that in a water Cherenkov detector (e.g. SuperK) it is difficult to reduce this background to a level below $\mathcal{O}(3\%)$ of the CC rate. A liquid argon detector is believed to provide much better π^0-electron discrimination, and will perhaps enable the π^0 background to be reduced to $\mathcal{O}(0.1\%)$ of the CC rate [70]. Based on these considerations there are two different detector strategies. We can choose a water Cherenkov detector, enabling us to maximize the detector mass, and hence the event statistics, but obliging us to tolerate a significant background from π^0 production in NC events. Alternatively, we can choose a detector technology that highly suppresses the π^0 background, but this will oblige us to use a smaller fiducial mass, and hence lower event statistics.

For a given choice of beamline design, baseline, and detector parameters, the experimental $\nu_\mu \to \nu_e$ and $\bar{\nu}_\mu \to \bar{\nu}_e$ sensitivities can be calculated. It is useful to define some representative scenarios, characterized by (a) the parameters of the primary proton beam incident on the pion production target, (b) the data sample size D (kt yr), defined as the product of the detector fiducial mass, the efficiency of the signal selection requirements, and the number of years of data taking, (c) the background fraction f_B defined as the background rate divided by the CC rate for events that survive the signal selection requirements, and (d) the fractional systematic uncertainty σ_{f_B}/f_B on the predicted f_B.

We will consider neutrino superbeams that can be produced with MW-scale proton beams at low energy ($E_\nu \sim 1$ GeV) at the proposed Japan Hadron Facility (JHF) and at high energy ($E_\nu \gtrsim 3$ GeV) at laboratories with high-energy proton drivers that might be upgraded to produce these superbeams (BNL, CERN, DESY, and Fermilab). For the sake of definiteness, in the following we will restrict our considerations to two explicit MW-scale primary proton beams. First, we will consider the 0.77 MW beam at the 50 GeV proton synchrotron of the proposed JHF, and a 4 MW upgrade which we refer to as SJHF (Superbeam JHF). Second, we consider a 1.6 MW proton driver upgrade that is under study at Fermilab. With this new proton driver, and modest upgrades to the 120 GeV Fermilab Main Injector (MI), it is possible to increase the beam current within the MI by a factor of 4, and hence increase the intensity of the NuMI beam by a factor of 4, which we refer to as SNuMI (Superbeam NuMI). Higher beam intensities are precluded by space-charge limitations in the MI [71]. For both the SJHF and SNuMI cases we will assume a run plan in which there is 3 years of data taking with a neutrino beam followed by 6 years of data taking with an antineutrino beam. In principle the high-energy superbeams could be produced at any of the present laboratories with high-energy proton drivers.

We define three aggressive detector scenarios, which are summarized in Table I:

Scenario A, which might be realized with a liquid argon detector. We choose a 30 kt fiducial mass, which has been considered previously for a neutrino factory detector. We assume tight selection requirements are used to suppress the π^0 background, and take the signal efficiency to be 0.5. This will result in $D = 45$ kt yr for neutrino running and 90 kt yr for antineutrino running. We assume that backgrounds from π^0 events contribute 0.001 to f_B [72], and the ν_e contamination in the beam contributes 0.003 to f_B in neutrino running, and 0.005 to f_B in antineutrino running. We neglect all other backgrounds. Hence, $f_B = 0.004$ (0.006) for neutrino (antineutrino) running. Finally, we will assume that we know the background rate with a precision of 10% ($\sigma_{f_B}/f_B = 0.1$).

Scenario F, which might be realized with a fine-grain iron sampling calorimeter. We choose a 10 kt fiducial mass, which is a factor of 10 larger than the THESEUS detector [73]. Since this fiducial mass is smaller than for the alternative scenarios we are considering, we will assume that the selection cuts are not tight, and that the selection efficiency is 0.9. This will result in $D = 27$ kt yr for neutrino running and

TABLE I. Parameters for scenarios A, F, and W discussed in the text. The scenarios assume 3 years of neutrino running and 6 years of antineutrino running. The data set sizes D and background fractions f_B are defined for the event samples after the signal selection requirements have been applied.

	Scenario A		Scenario F		Scenario W	
	ν	$\bar{\nu}$	ν	$\bar{\nu}$	ν	$\bar{\nu}$
Fiducial mass (kt)	30	30	10	10	220	220
D (kt yr)	45	90	27	54	450	900
Backg. frac. f_B	0.004	0.006	0.013	0.015	0.02	0.02
Backg. uncertainty σ_{f_B}/f_B	0.1	0.1	0.1	0.1	0.1	0.1

54 kt yr for antineutrino running. We assume that backgrounds from π^0 events contribute 0.01 to f_B, and the ν_e contamination in the beam contributes 0.003 to f_B in neutrino running, and 0.005 to f_B in antineutrino running. We neglect all other backgrounds. Hence, $f_B=0.013$ (0.015) for neutrino (antineutrino) running. Finally, we will assume that we know the background rate with a precision of 10% ($\sigma_{f_B}/f_B=0.1$).

Scenario W, which might be realized for a low-energy beam with a water Cherenkov detector. We choose a 220 kt fiducial mass, a factor of 10 larger than the SuperK detector. Guided by the study described in Ref. [68] we will assume the selection requirements used to suppress the π^0 background result in a signal efficiency of 0.68. This will result in $D=450$ kt yr for neutrino running and 900 kt yr for antineutrino running. We assume that backgrounds from π^0 events dominate, and set $f_B=0.02$. Note that a detailed detector simulation has obtained $f_B=0.03$ for a water Cherenkov detector at a low energy NBB at the JHF [68]. With further optimization the choice $f_B=0.02$ might therefore be realizable at low energy, but for higher energy (>1 GeV) neutrino beams the rejection against the π^0 background is expected to be much worse. Hence, a new detector technology might be required for this scenario to make sense at high energies. Finally, we will assume that we know the background rate with a precision of 10% ($\sigma_{f_B}/f_B=0.1$).

Scenarios A, F, and W are very aggressive, and may or may not be realizable in practice. In the following we will explore the oscillation sensitivity as a function of D, f_B, σ_{f_B}/f_B, baseline, and neutrino beam energy. Scenario F is clearly inferior to scenario A, which has larger D and smaller f_B. Therefore, in the following we will not discuss the scenario F physics potential in detail, but we will indicate the scenario F physics potential on several relevant figures. We will use scenarios A and W extensively to illustrate the physics potential of upgraded conventional neutrino beams, and facilitate a discussion of the challenges involved in probing small values of $\sin^2 2\theta_{13}$.

IV. $\sin^2 2\theta_{13}$ REACH

For a given neutrino beam, baseline, and detector, we wish to calculate the resulting $\sin^2 2\theta_{13}$ reach, which we define as the value of $\sin^2 2\theta_{13}$ that would result in a $\nu_\mu \to \nu_e$ or $\bar{\nu}_\mu \to \bar{\nu}_e$ signal that is 3 standard deviations above the background. In our analysis we will take into account the Poisson

statistical uncertainties in the numbers of signal and background events, and the systematic uncertainty on the background subtraction. Our prescription for determining the $\sin^2 2\theta_{13}$ reach is given in the Appendix. In the following, unless otherwise stated, the $\sin^2 2\theta_{13}$ reaches are calculated setting the sub-leading oscillation parameters $\sin^2 2\theta_{12}=0.8$ and $\delta m_{21}^2=10^{-5}$ eV^2. The small δm_{21}^2 effectively switches off contributions from the sub-leading scale. Larger values of δm_{21}^2 can yield contributions to the $\nu_\mu \to \nu_e$ signal, but these contributions are not important unless $\sin^2 2\theta_{13}$ is significantly less than 10^{-3}.

A. Sensitivity at the Japan Hadron Facility

The Japan Hadron Facility working group has recently investigated [68] the $\nu_\mu \to \nu_e$ oscillation sensitivity attainable at the proposed 0.77 MW 50 GeV proton synchrotron in Japan, using a 295 km baseline together with the SuperK detector. In their study they considered a variety of low energy ($\langle E_\nu \rangle \sim 1$ GeV) WBB and NBB beamline designs. The resulting experimental scenario is similar to the one later considered in Ref. [33]. The conclusions from the study were the following: (i) With a water Cherenkov detector the sensitivity is limited by the π^0 background produced in NC events. To minimize the background a NBB must be used, since in a WBB the high energy tail will be the dominant source of background events. (ii) With an effective $\nu_\mu \to \nu_e$ oscillation amplitude of $\sin^2 2\theta_{\mu e}=0.05$ at an oscillation scale of $\delta m_{32}^2=0.003$ eV^2, the best set of selection requirements identified in the study yielded $f_B=0.03$, and a signal:background ratio of 1:1 with 12.3 signal events per year in the SuperK detector. A 10% systematic uncertainty on the background rate was assumed. If no signal is observed after 5 years of running, the expected limit would be $\sin^2 2\theta_{\mu e}<0.01$ at 90% C.L., which corresponds to a $\sin^2 2\theta_{13}$ reach of 0.05. (iii) With a detector of mass 20 × SuperK, after 5 years running the resulting limit in the absence of a signal would be $\sin^2 2\theta_{\mu e}<0.003$ at 90% C.L., which corresponds to a $\sin^2 2\theta_{13}$ reach of 0.01. (iv) The energy distribution of the background events is similar to the corresponding distribution for the signal. Hence, the $\nu_\mu \to \nu_e$ search is essentially a counting experiment. Using these JHF study results, we find that the appropriate values to use in evaluating the $\sin^2 2\theta_{13}$ reach for the JHF to SuperK experiment are $f_B=0.03$, $\sigma_{f_B}/f_B=0.1$, and $D=75$ kt-years (SuperK with 5 years exposure and a signal efficiency of 68%). With these values,
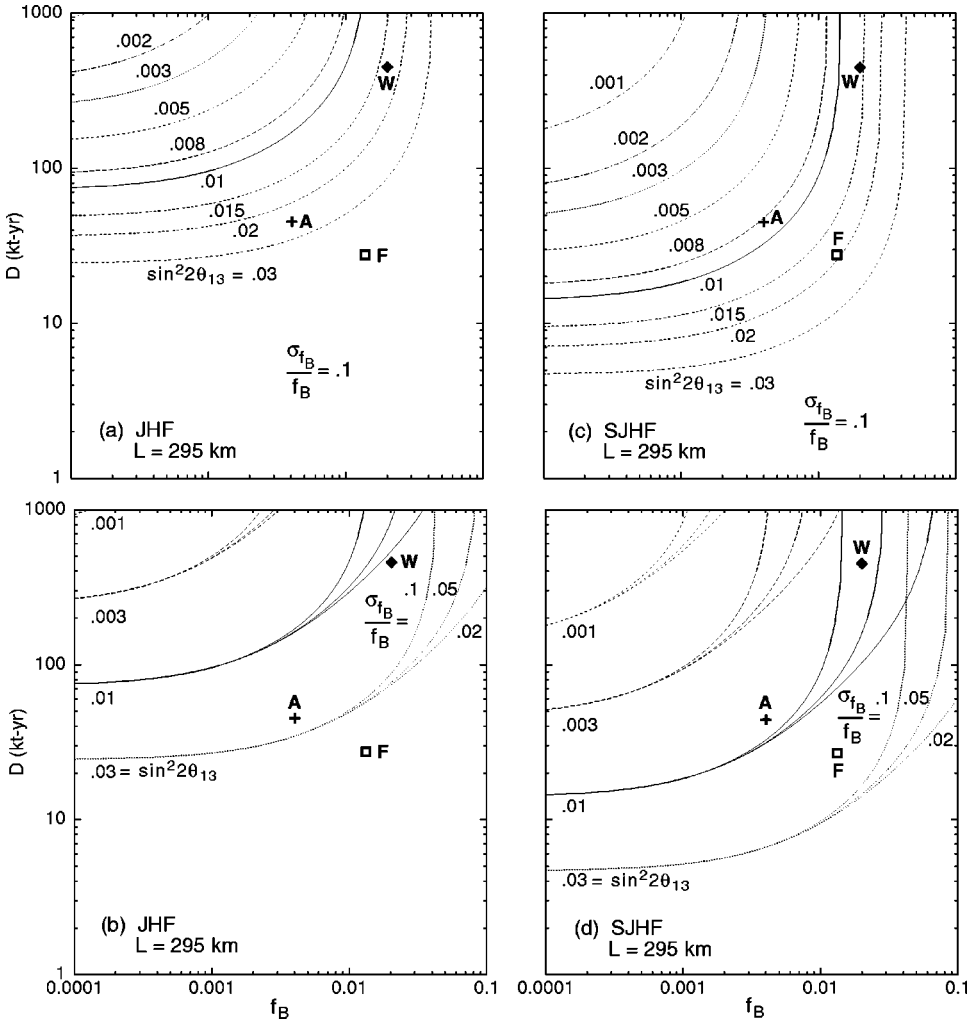
FIG. 1. Contours of constant $\sin^2 2\theta_{13}$ reach that correspond to a $\nu_e \rightarrow \nu_\mu$ signal that is 3 standard deviations above the background. The contours are shown in the (D, f_B) plane, where D is the data-sample size and f_B the background rate divided by the total CC rate. The contours are shown for the 0.77 MW (left-hand plots) and 4.0 MW (right-hand plots) JHF scenarios with $L = 295$ km. The top panels show curves for $\sigma_{f_B}/f_B = 0.1$, while the bottom panels show curves for $\sigma_{f_B}/f_B = 0.1$, 0.05, and 0.02. The positions corresponding to the three standard detector scenarios defined in Table I are indicated.

our statistical treatment recovers the 90% C.L. results presented in the JHF report [68]. In our calculations for SJHF we used the neutrino intraction rates presented in Ref. [68].

We can now investigate the dependence of the $\sin^2 2\theta_{13}$ reach on the detector parameters, and hence try to understand whether a massive water Cherenkov detector is likely to be the best option. In Fig. 1 contours of constant $\sin^2 2\theta_{13}$ reach are shown as a function of the dataset size D and the background rate f_B for 3 years of running at the 0.77 MW JHF beam (left-hand plots) and at an upgraded 4 MW SJHF beam (right-hand plots). The lower panels show how the $\sin^2 2\theta_{13}$ reach varies with σ_{f_B}/f_B. The contours have a characteristic shape. At sufficiently large D the $\sin^2 2\theta_{13}$ sensitivity is limited by the systematic uncertainties associated with the background subtraction, and the reach does not significantly improve with increasing dataset size. The contours are therefore vertical in this region of Fig. 1. At sufficiently small D the sensitivity of the $\nu_\mu \rightarrow \nu_e$ appearance search is limited by signal statistics, and further reductions in f_B do not improve the $\sin^2 2\theta_{13}$ reach. The contours are therefore horizontal in this region of Fig. 1. The positions in the (f_B, D) plane corresponding to our three detector scenarios (A, F, and W) are indicated on the figure. For the 0.77 MW machine the two scenarios (A and W) both yield reaches in the range

$\sin^2 2\theta_{13} \sim 0.015$ to 0.03. However, the water Cherenkov sensitivity is limited by the systematic uncertainty in the substantial π^0 background. Hence, the $\sin^2 2\theta_{13}$ reach for scenario W does not improve substantially when the accelerator beam is upgraded from 0.77 MW to 4 MW (SJHF). On the other hand, this upgrade would result in a substantial improvement in the reach obtained with scenario A, which is not background limited, and therefore has a reach improving almost linearly with D. We conclude that, even with SJHF, it will be difficult to observe a $\nu_\mu \rightarrow \nu_e$ signal if $\sin^2 2\theta_{13}$ is less than about 0.01. This conclusion is consistent with the JHF study group analysis, but is in conflict with the expectations of Ref. [33]. On the positive side, if $\sin^2 2\theta_{13}$ is larger than 0.01, a 1 GeV neutrino beam at JHF or SJHF would permit the observation of a $\nu_\mu \rightarrow \nu_e$ signal. Detector scenario W does slightly better for a 0.77 MW JHF, while scenario A does slightly better for a 4.0 MW SJHF.

Finally, we consider whether the $\sin^2 2\theta_{13}$ reach at a 1 GeV JHF or SJHF neutrino beam can be improved with a different choice of baseline. Contours of constant reach in the (L, D) plane are shown for scenarios A and W in Fig. 2. A baseline of 295 km does indeed yield the optimal reach for the water Cherenkov scenario. For scenario A, a slightly shorter baseline (200 km) would yield a slightly improved reach.
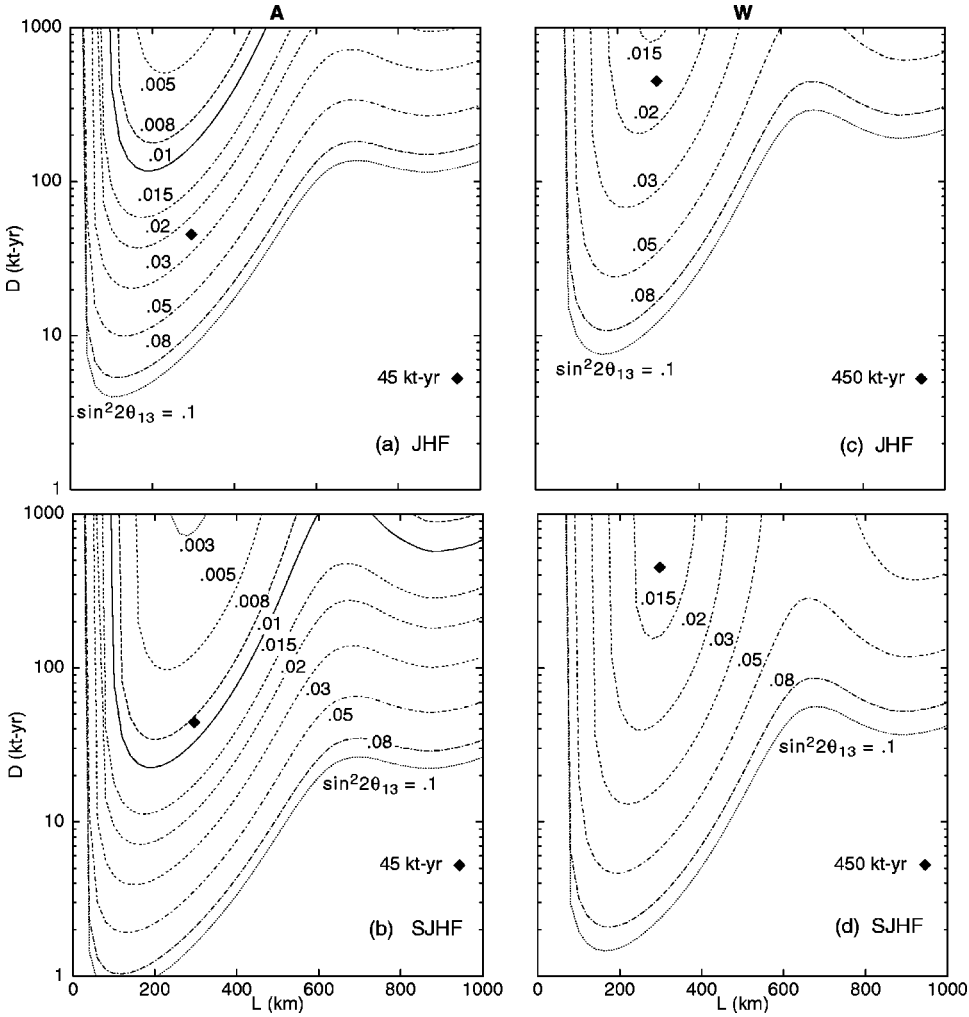
FIG. 2. Contours of constant $\sin^2 2\theta_{13}$ reach that correspond to a $\nu_e \rightarrow \nu_\mu$ signal that is 3 standard deviations above the background. The contours are shown in the (D,L) plane, where D is the data-sample size and L the baseline. The panels show predictions for the JHF scenario described in the text, for detector scenarios A (left-hand plots) and W (right-hand plots), and for 0.77 MW (top plots) and 4.0 MW (bottom plots) proton drivers. The positions corresponding to scenarios A and W (see Table I) at $L=295$ km are indicated.

B. Sensitivities for long baseline experiments

1. Decay channel length restrictions

Consider next the sensitivity that can be achieved with longer baselines and higher energies. We begin by considering how restrictions on the decay channel length reduce the neutrino flux for very long baselines. In a conventional neutrino beamline design it is desirable that the pion decay channel is long enough for most of the pions to decay. However, for very long-baseline experiments the decay channel must point downwards at a steep angle, and the geology under the accelerator site may impose significant constraints on the maximum length of the decay channel. In practice, an upgraded long-baseline conventional neutrino beam would be sited at an existing particle physics laboratory having a high-energy proton accelerator: Brookhaven or Fermilab in the U.S., CERN or DESY in Europe, or the planned JHF laboratory in Japan. The rock characteristics under the JHF site are expected to be determined next year by drilling [70]. The site with the deepest viable rock layer in the U.S. is Fermilab, which sits above approximately 200 m of good rock. The Brookhaven and DESY [74] laboratories sit just above the water table—an impediment that would have to be overcome before a high-energy long-baseline beam could be proposed. The depth of the good rock (Molasse) under CERN

varies between about 200 m and 400 m, depending on location [72]. The impact of these restrictions on the maximum decay channel length is shown as a function of the baseline length in Fig. 3 for the Fermilab and CERN sites. The resulting fraction of pions that decay within the decay channel is summarized in Table II for several neutrino beam energies. The channel length calculations were performed assuming that (i) the proton accelerator is at a depth of 10 m, (ii) the beam is then bent down to point in the appropriate baseline-dependent direction using a magnetic channel with an average field of 2 Tesla, and (iii) once pointing in the right direction the proton beam enters a 50 m long targeting and focusing section, after which the decay channel begins. The maximum decay channel length then depends upon whether the channel extends all the way to the bottom of the usable rock layer or whether this rock layer must also accommodate a near detector. Results for both of these cases are presented in Fig. 3 and Table II. In the near-detector case the maximum decay channel length has been reduced by 100 m to allow for the shielding and detector hall. The pion decay fraction estimates have been made assuming that all of the decaying pions have the average pion energy in the channel.

The decay fractions in Table II show that the site-dependent depth restrictions will result in a significant reduc-
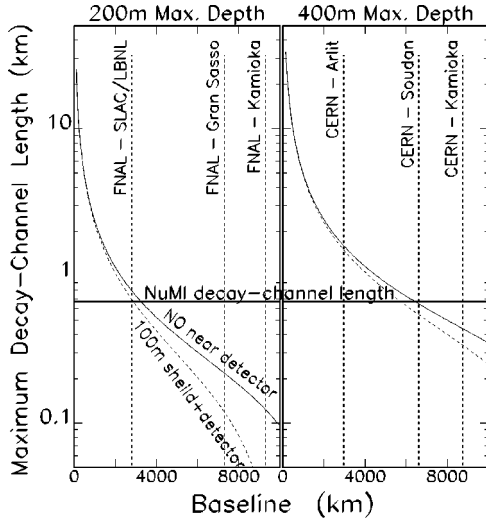
FIG. 3. Maximum length of the pion decay channel that fits within a rock layer that is 200 m deep (left-hand plot) and 400 m deep (right-hand plot) shown as a function of baseline. The calculation is described in the text. The solid (dashed) curves shows the results without (with) a near detector. For comparison, the horizontal solid line indicates the NuMI decay channel length.

tion in the neutrino beam intensities for high-energy long-baseline beams. For example, at the Fermilab site there is no room for a near detector if the baseline is 9300 km (Fermilab to SuperK). With the medium energy beam and a baseline of

TABLE II. The fraction of pions decaying in a channel with the maximum length permitted by the depth of viable rock (D_{max}) under the accelerator site, tabulated as a function of baseline L for configurations with and without a near detector.

SNuMI Beam	E_ν(peak) (GeV)	D_{max} (m)	L (km)	f_{decay} With near	no near
LE	3	200	2900	0.93	0.95
			7300	0.36	0.56
			9300	—	0.37
ME	7	200	2900	0.67	0.72
			7300	0.17	0.29
			9300	—	0.17
HE	15	200	2900	0.41	0.44
			7300	0.09	0.16
			9300	—	0.09
LE	3	400	2900	0.98	0.99
			7300	0.82	0.88
			9300	0.67	0.77
ME	7	400	2900	0.93	0.94
			7300	0.56	0.64
			9300	0.38	0.47
HE	15	400	2900	0.69	0.72
			7300	0.29	0.34
			9300	0.20	0.26

TABLE III. $\sin^2 2\theta_{13}$ reach (corresponding to a signal that is 3 standard deviations above the background after 3 years of running with a neutrino superbeam) shown as a function of baseline L for scenario A described in the text. The oscillation probability $P(\nu_\mu \rightarrow \nu_e)$ corresponding to $\sin^2 2\theta_{13} = 0.01$ and the expected numbers of signal events S and background events B are also listed. The calculations assume $\Delta m^2_{32} = 3.5 \times 10^{-3}$ eV^2, $\delta m^2_{21} = 5 \times 10^{-5}$ eV^2, and $\delta = 0$.

SNuMI Beam	E_ν(peak) (GeV)	L (km)	P	S	B	$\sin^2 2\theta_{13}$ reach
LE	3	730	0.0024	210	340	0.006
		2900	0.0045	26	24	0.008
		7300	0.012	4.1	1.3	0.02
		9300[a]	0.016	3.2	0.8	0.02
ME	7	730	0.0016	370	910	0.01
		2900	0.0075	120	62	0.003
		7300	0.025	15	2.4	0.006
		9300[a]	0.035	14	1.6	0.006
HE	15	730	0.0006	290	2000	0.02
		2900	0.0054	180	130	0.003
		7300	0.024	25	4.2	0.004
		9300[a]	0.032	25	3.1	0.004

[a]No near detector.

7300 km (Fermilab to Gran Sasso) only 17% of the pions decay within the channel. Hence, the channel length restrictions would exclude, or at least heavily penalize, the extremely long baseline ideas proposed by Dick *et al.* [75]. Clearly, decay channel length restrictions must be taken into account when comparing choices of baseline and beam energy.

2. $\sin^2 2\theta_{13}$ reach for scenarios A and W

We are now ready to consider the $\sin^2 2\theta_{13}$ reach that can be obtained in a long-baseline experiment. In our main discussion we consider $\nu_e \rightarrow \nu_\mu$ appearance with $\delta m^2_{32} > 0$; the $\delta m^2_{32} < 0$ case is discussed at the end of this section. Our calculations use the WBB spectra and interaction rates presented in the MINOS design report [14] for the low-energy (LE) horn configuration ($E_\nu \sim 3$ GeV), the medium-energy (ME) horn configuration ($E_\nu \sim 7$ GeV), and the high-energy (HE) horn configuration ($E_\nu \sim 15$ GeV). After accounting for the decay channel length restrictions arising from a maximum depth requirement of 200 m, the neutrino fluxes are assumed to scale with the inverse square of the baseline length.

The calculated reaches are listed in Tables III and IV for detector scenarios A and W, and several baselines: $L = 730$ km (Fermilab→Soudan or CERN→Gran Sasso), $L = 2900$ km (Fermilab→LBNL/SLAC), $L = 7300$ km (Fermilab →Gran Sasso), and $L = 9300$ km (Fermilab→SuperK). Note that the shortest baseline (730 km) has a very limited $\sin^2 2\theta_{13}$ reach for all the beams, and the lowest energy beam (LE) has a very limited $\sin^2 2\theta_{13}$ reach for all baselines. The best reach for detector scenario A is $\sin^2 2\theta_{13} = 0.003$, which is obtained with a baseline that is not too long (e.g. 2900

TABLE IV. $\sin^2 2\theta_{13}$ reach (corresponding to a signal that is 3 standard deviations above the background after 3 years of running with a neutrino superbeam) shown as a function of baseline L for Scenario W described in the text. The oscillation probability $P(\nu_\mu \rightarrow \nu_e)$ corresponding to $\sin^2 2\theta_{13}=0.01$, and the expected numbers of signal events S and background events B are also listed. The calculations assume $\Delta m^2_{32}=3.5\times 10^{-3}$ eV^2, $\delta m^2_{21}=5\times 10^{-5}$ eV^2, and $\delta=0$.

SNuMI Beam	E_ν(peak) (GeV)	L (km)	P	S	B	$\sin^2 2\theta_{13}$ reach
LE	3	730	0.0024	2100	17000	0.03
		2900	0.0045	260	1200	0.02
		7300	0.012	41	67	0.009
		9300[a]	0.016	32	40	0.008
ME	7	730	0.0016	3700	46000	0.05
		2900	0.0075	1200	3100	0.008
		7300	0.024	150	120	0.003
		9300[a]	0.035	140	80	0.003
HE	15	730	0.0006	2900	98000	0.1
		2900	0.0054	1800	6700	0.01
		7300	0.024	250	210	0.003
		9300[a]	0.032	250	160	0.003

[a]No near detector.

km). The best reach for detector scenario W is also $\sin^2 2\theta_{13}=0.003$, and is obtained with long baselines (e.g. 7300 km or 9300 km) which benefit from the enhancement of the oscillation amplitude due to matter effects. The reaches for the two longest baselines are about the same since the increase of the matter enhancement as L increases is compensated by the decrease in the pion decay fraction due to the decay channel length restriction.

To further illustrate the impact of the decay channel length restrictions on the $\sin^2 2\theta_{13}$ reach for long-baseline experiments, in Fig. 4 contours of constant reach are shown in the (f_B,D) plane for $L=7300$ km with the channel length restrictions (right-hand plots) and without the channel length restrictions (left-hand plots). The scenario W point lies in the systematics-dominated (vertical contour) region, and is therefore not significantly affected by a reduction in D due to the decay channel length restrictions. However, the scenario A point lies between the systematics-limited and statistics-limited regions of the plot, and is significantly affected by the reduction in neutrino flux due to the channel length restrictions. Indeed, in scenario A the $\sin^2 2\theta_{13}$ reach at the HE beam is degraded from about 0.0015 to about 0.004 by the channel length restriction.

3. Dependence on detector parameters

We can now explore the dependence of the $\sin^2 2\theta_{13}$ reach on the baseline, beam energy, and detector parameters. In Fig. 5 contours of constant $\sin^2 2\theta_{13}$ reach are shown in the (f_B,D) plane for $L=730$ km and 2900 km. As already noted, for our detector scenarios A and W the best reach is ~ 0.003, obtained with scenario A at $L=2900$ km using either the ME or HE beams (Figs. 5e and 5f) or with scenario

W at $L=7300$ km using the same beams (Figs. 4e and 4f). It is interesting to consider what improvements to scenarios A and W would be required to obtain a reach of 0.001, for example. This goal can be attained by decreasing the background fraction f_B for scenario W to $f_B \sim 0.004$ (or alternatively increasing the dataset size D for scenario A by a factor of 10) and using the HE beam at a very long baseline. The goal could also be attained by decreasing f_B for scenario A by an order of magnitude and using the high energy beam and a baseline of 2900 km, for example. None of these revised detector scenarios seems practical. An alternative strategy is to try to find a detector scenario with a smaller systematic uncertainty on f_B. Figure 6 shows, for the ME and HE beams, contours of constant $\sin^2 2\theta_{13}$ reach in the (f_B,D) plane for several different σ_{f_B}/f_B, and for baselines of 2900 km, 4000 km, and 7300 km. The scenario W sensitivity would benefit if the systematic uncertainty in the background could be reduced, but even a factor of 5 improvement in σ_{f_B}/f_B would not permit a reach of 0.001 to be attained.

Since detector scenarios A and W are ambitious, we can ask what happens if D, f_B, or σ_{f_B}/f_B must be relaxed. The best reaches obtained with scenario W were for the ME and HE beams at very long baselines (e.g. $L=7300$ km). In these cases the reach is not very sensitive to D, but degrades roughly linearly with increasing f_B (Fig. 4) or σ_{f_B}/f_B (Fig. 6). Hence, if the achievable background rate is really $f_B=0.1$, then the $\sin^2 2\theta_{13}$ reach is well above 0.01 for the observation of a $\nu_\mu \rightarrow \nu_e$ signal at 3 standard deviations above the background. The best reaches obtained with scenario A were for the ME and HE beams at long baselines (e.g. $L=2900$ km). In these cases the reach is sensitive to both decreases in D and increases in f_B. The reach can be degraded by a factor of 2 by either reducing D by about a factor of 4 or by increasing f_B by about a factor of 3 (Fig. 5).

So far we have considered only a few discrete baseline lengths. To explore the reach that can be obtained with other baseline choices, Fig. 7 shows, for each of the three NuMI beam energies, contours of constant $\sin^2 2\theta_{13}$ reach in the (L, D) plane for scenarios A and W. For scenario A, where backgrounds are less important, the optimal distance varies with beam energy; crudely speaking, the optimal L is given by making the vacuum oscillation argument $1.27\delta m^2_{32}L/\langle E_\nu \rangle$ of order $\pi/2$. For scenario W the backgrounds are more important and larger distances give a better $\sin^2 2\theta_{13}$ reach for all three upgraded NuMI beams.

Finally, we have also studied neutrino beams with higher energy than NuMI. For example, the CNGS beam [76] at CERN has an average neutrino energy of about 20 GeV. We find that for the expected 3×10^{19} protons on target per year, three years of running will at best give a $\sin^2 2\theta_{13}$ reach of about 0.01 for either scenario A or W. Upgrading the proton intensity by a factor of four improves the $\sin^2 2\theta_{13}$ reach to about 0.005. Therefore we conclude that the higher-energy CNGS superbeams have similar capability to the SNuMI beams.

4. Summary of $\sin^2 2\theta_{13}$ reaches for $\delta m^2_{32}>0$ and $\delta m^2_{32}<0$

In summary, Figs. 4, 5, and 7 show that the best $\sin^2 2\theta_{13}$ reach that can be obtained with detector scenarios A and W is
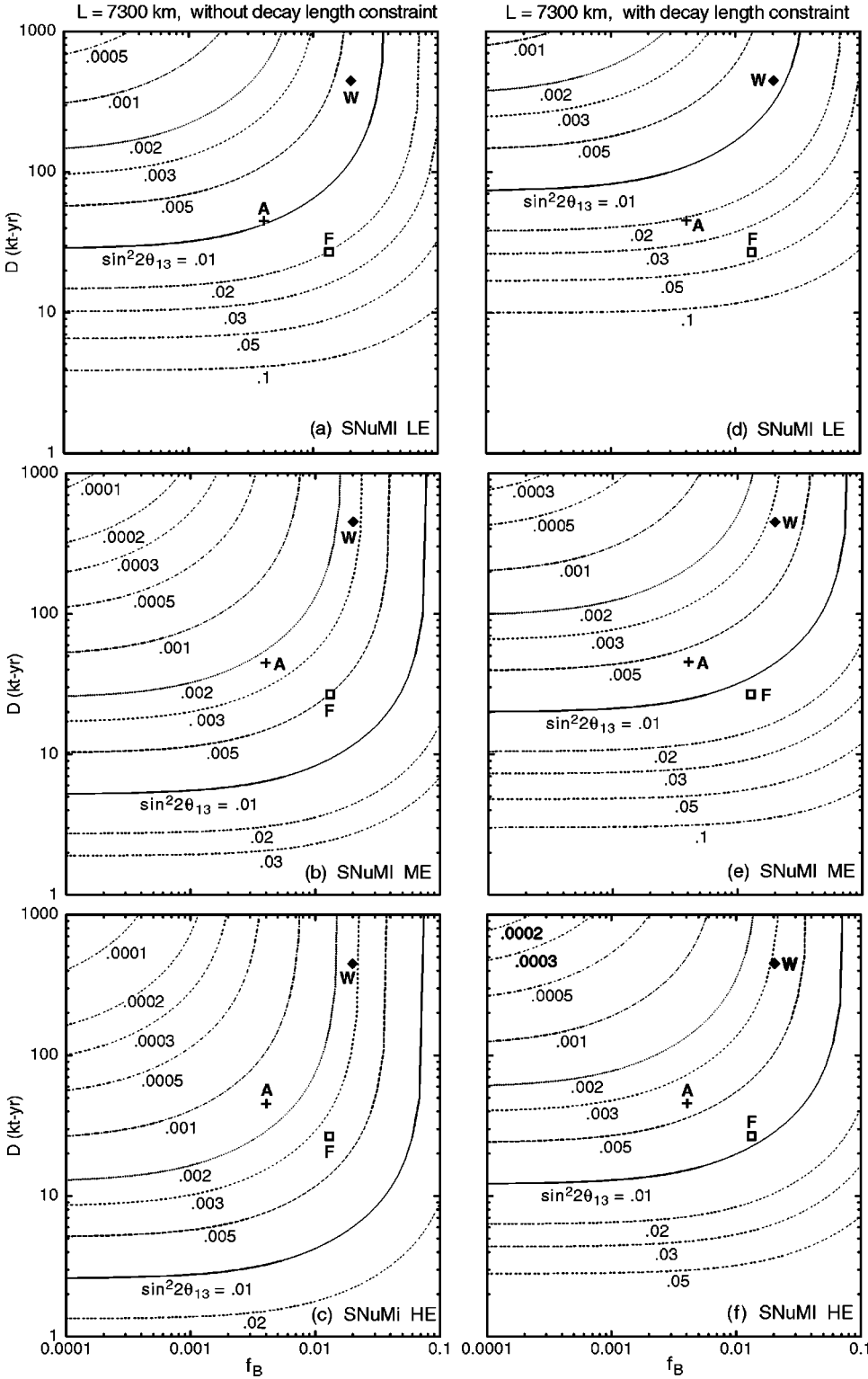
FIG. 4. Contours of constant $\sin^2 2\theta_{13}$ reach that correspond to a $\nu_e \rightarrow \nu_\mu$ signal that is 3 standard deviations above the background, at $L = 7300$ km. The contours are shown in the (D, f_B) plane, where D is the data-sample size and f_B the background rate divided by the total CC rate. The contours are shown for the LE (top plots), ME (center plots), and HE (lower plots) upgraded SNuMI beams, both with (right plots) and without (left plots) the decay length constraint. The systematic uncertainty $\sigma_{f_B}/f_B = 0.1$. The positions corresponding to the three standard scenarios defined in Table I are indicated.

about 0.003. This optimum reach can be obtained in scenario A with $L \sim 2000-4000$ km for the NuMI ME beam or with $L \sim 3000-6000$ km for the HE beam, or in scenario W with $L \sim 7000-9000$ km for either the ME or HE beams. Scenarios A and W require ambitious detector parameters. To improve the reach to 0.001, for example, requires substantial improvements in f_B, σ_{f_B}/B, and/or D, and does not therefore seem practical. If the scenario A and W parameters can-

not be realized the reach will be degraded. In particular, a significant increase of f_B (or σ_{f_B}/f_B) in either scenario A or W would result in a significant decrease in $\sin^2 2\theta_{13}$ reach. A significant decrease in the data-sample size in scenario A will also degrade the $\sin^2 2\theta_{13}$ reach.

Up to now we have considered the sensitivity of long baseline experiments if $\delta m_{32}^2 > 0$. We now turn our attention to the alternative case: $\delta m_{32}^2 < 0$. In this case long baseline
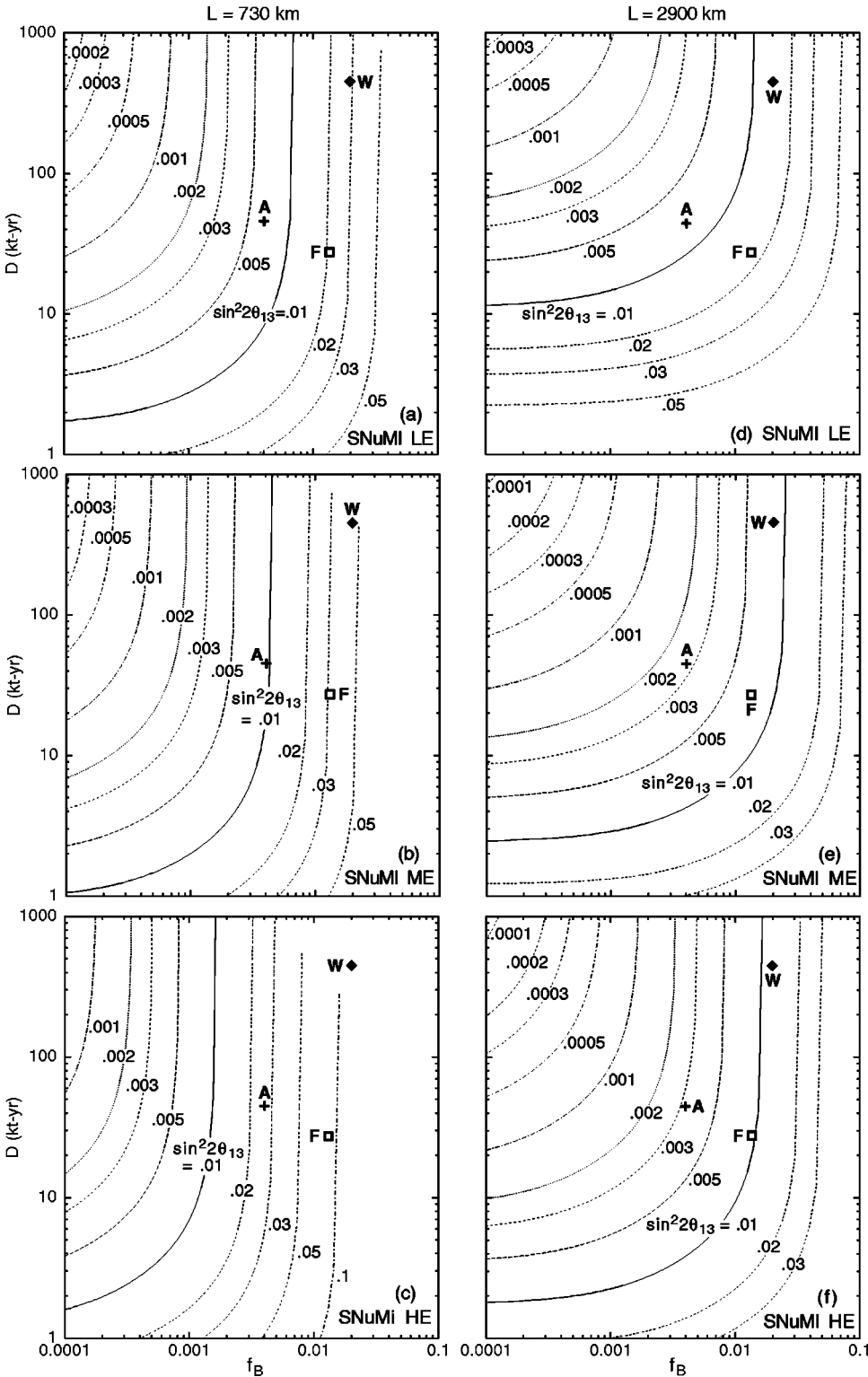
FIG. 5. Contours of constant $\sin^2 2\theta_{13}$ reach that correspond to a $\nu_e \rightarrow \nu_\mu$ signal that is 3 standard deviations above the background, at $L = 730$ km (left plots) and 2900 km (right plots). The contours are shown in the (D, f_B) plane, where D is the data-sample size and f_B the background rate divided by the total CC rate. The contours are shown for the LE (top plots), ME (center plots), and HE (lower plots) upgraded SNuMI beams. The systematic uncertainty in the background subtraction is $\sigma_{f_B}/f_B = 0.1$. The positions of the three standard scenarios defined in Table I are indicated.

experiments using a neutrino beam will suffer from a suppression of signal due to matter effects. Therefore, in our scenarios A and W, if no signal is observed after 3 years of neutrino running the beam is switched to antineutrinos for a further 6 years of data taking. For antineutrino running with $\delta m_{32}^2 < 0$ the results shown in Figs. 4, 5, and 7 must be modified since the antineutrino cross section is about half of the neutrino cross section. Hence we must double the required

values on the D axes in the various figures. Other modifications to the contour plots for antineutrino running with $\delta m_{32}^2 < 0$ are minor since the matter enhancement in this case is similar to the enhancement for neutrinos when $\delta m_{32}^2 > 0$ (they are the same in the limit that the sub-leading oscillation can be ignored). However, the positions of the scenario A and W points on the various figures must be moved to account for the larger values of D and f_B (and potentially
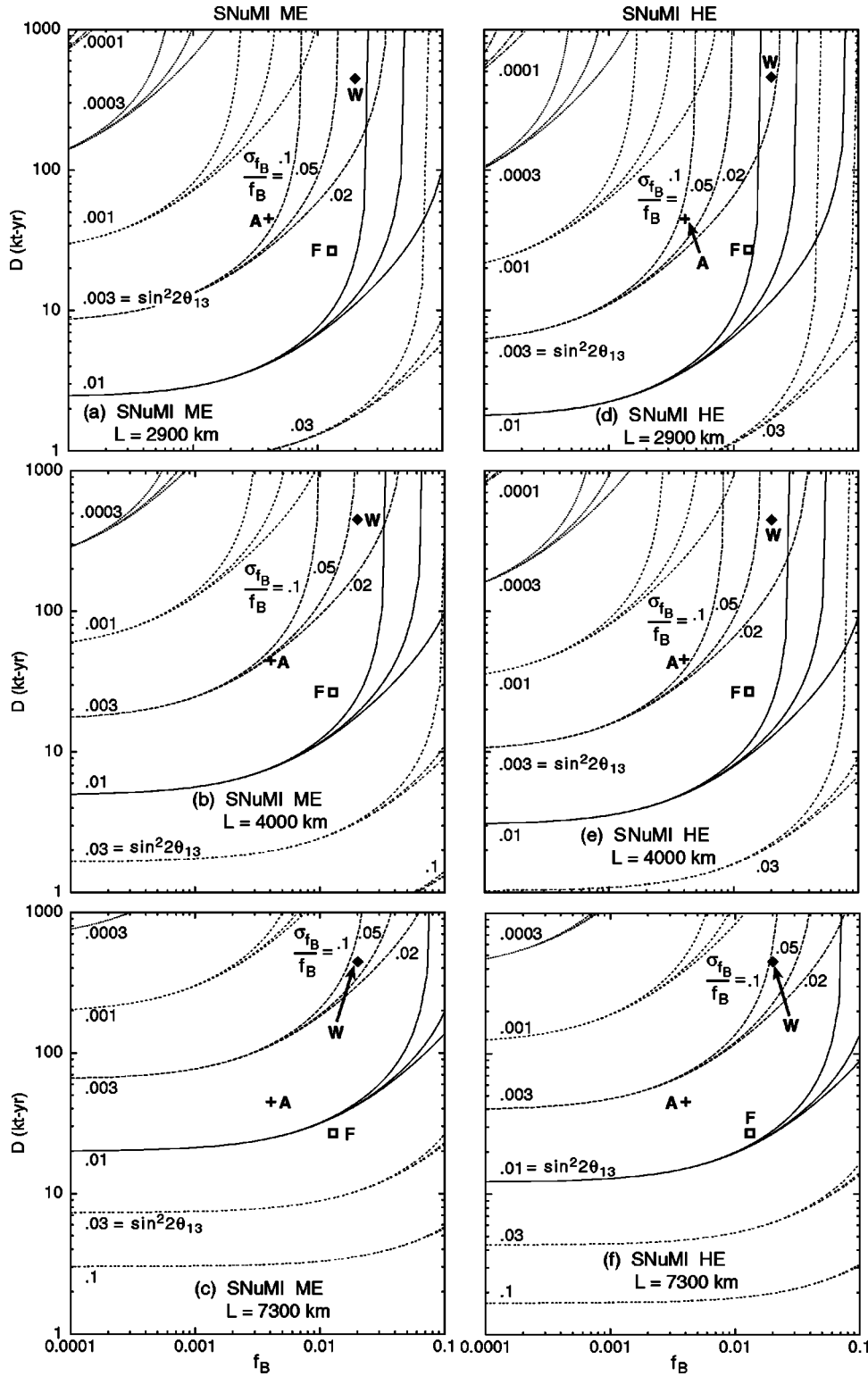
FIG. 6. Contours of constant $\sin^2 2\theta_{13}$ reach that correspond to a $\nu_e \rightarrow \nu_\mu$ signal that is 3 standard deviations above the background, at the upgraded SNuMI ME (left) and HE (right) beams. The contours are shown in the (D, f_B) plane, where D is the data-sample size and f_B the background rate divided by the total CC rate. The contours are shown for $L=2900$ (top), 4000 (center), and 7300 km (bottom). Curves are shown for systematic uncertainties on the background subtraction $\sigma_{f_B}/f_B = 0.1$, 0.05, and 0.02. The positions of the three standard scenarios defined in Table I are indicated. The decay length constraints have been imposed for $L=4000$ and 7300 km.

σ_{f_B}/f_B). Note that the larger background rate associated with antineutrino running in scenario A will degrade the ultimate $\sin^2 2\theta_{13}$ reach for $\delta m^2_{32} < 0$; the best reach becomes ~ 0.004.

V. NEUTRINO MASS HIERARCHY AND CP VIOLATION

In the 1 GeV and multi-GeV superbeam scenarios that we have considered it will be difficult to observe a $\nu_\mu \rightarrow \nu_e$ or $\bar{\nu}_\mu \rightarrow \bar{\nu}_e$ signal if $\sin^2 2\theta_{13}$ is smaller than about 0.01. However, if $\sin^2 2\theta_{13}$ is $\mathcal{O}(0.01)$, a $\nu_\mu \rightarrow \nu_e$ signal would be observable provided a sufficiently massive detector with sufficiently small background is practical. We would like to know if, in this case, the sign of δm^2_{32} can be determined in the long-baseline multi-GeV beam experiment and whether CP violation might be observed in either the long-baseline multi-GeV beam experiment or the 1 GeV intermediate
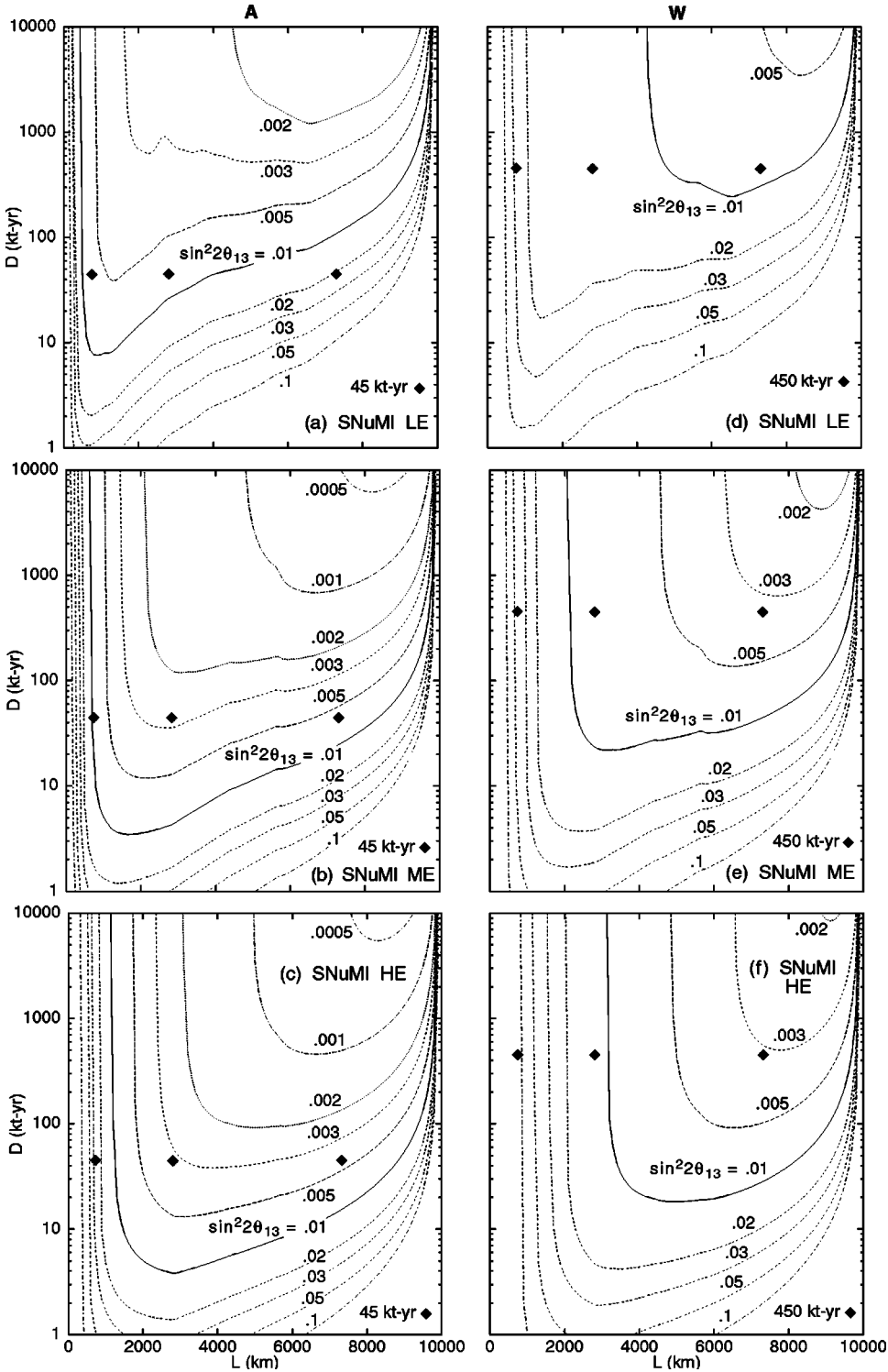
FIG. 7. Contours of constant $\sin^2 2\theta_{13}$ reach that correspond to a $\nu_e \rightarrow \nu_\mu$ signal that is 3 standard deviations above the background. The contours are shown in the (D,L) plane, where D is the data-sample size and L the baseline. The panels show predictions for the upgraded SNuMI LE (top), ME (center), and HE (bottom) beams, and for detector scenarios A (left plots) and W (right plots). The decay length constraint is included. The systematic uncertainty in the background subtraction $\sigma_{f_B}/f_B = 0.1$. The positions of the standard scenarios defined in Table I are shown at $L=730$, 2900, and 7300 km.

baseline experiment. We begin by considering the CP sensitivity at the SJHF, and then consider the sensitivity for determining CP violation and/or the pattern of neutrino masses at long baselines.

A. *CP* violation with a JHF superbeam

In our SJHF scenario, a CP violation search would consist of running for 3 years with a neutrino beam and measuring the number of $\nu_\mu \rightarrow \nu_e$ signal events $[N(e-)]$, and then running for 6 years with an antineutrino beam and measuring the number of $\bar{\nu}_\mu \rightarrow \bar{\nu}_e$ signal events $[N(e+)]$. In our calculations we assume that the antineutrino cross section is about one-half of the neutrino cross section, and that the antineutrino flux is the same as the neutrino flux. In the absence of CP violation ($\delta=0$ or $180°$), after correcting for cross-section and flux differences, we would therefore expect $N(e+) \simeq N(e-)$. In the presence of maximal CP violation
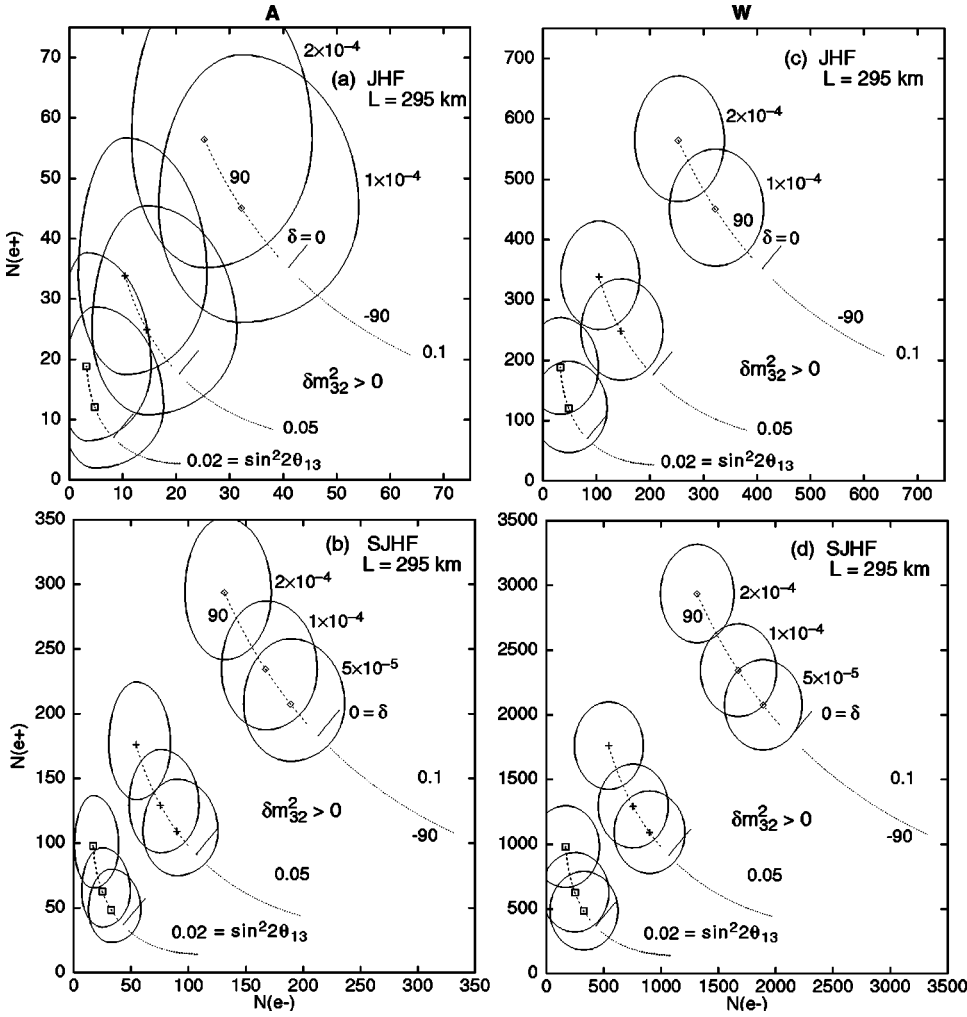
FIG. 8. 3σ error ellipses in the $[N(e^+),N(e^-)]$ plane, shown for the 0.77 MW JHF (top plots) and 4 MW SJHF (bottom plots) scenarios with at $L=295$ km. The contours are shown for detector scenarios A (left) and W (right), with $\sin^2 2\theta_{13}=0.02$, 0.05, and 0.1. The solid (dashed) [dotted] curves correspond to $\delta=0°$ (90°) $[-90°]$ with δm_{21}^2 varying from 2×10^{-5} eV^2 to 2×10^{-4} eV^2. The error ellipses are shown for three simulated data points at $\delta m_{21}^2=5\times10^{-5}$, 10^{-4} and 2×10^{-4} eV^2.

with $\delta=90°[-90°]$ we would expect $N(e+)>N(e-)$ $[N(e+)<N(e-)]$. The magnitude of the deviation from $N(e+)=N(e-)$ induced by CP violation is quite sensitive to the sub-leading scale δm_{21}^2. Setting $\delta=90°$, in Fig. 8 the predicted positions in the $[N(e-),N(e+)]$ plane are shown for scenarios A (left-hand plots) and W (right-hand plots). The predictions are shown as a function of both $\sin^2 2\theta_{13}$ and δm_{21}^2. The error ellipses around each point indicate the measurement precision at 3 standard deviations, taking into account both statistical and systematic uncertainties, and using the statistical prescription described in the Appendix. An overall normalization uncertainty (which could account for uncertainties in the flux and/or cross sections) of 2% is included, although its effects are generally small. CP violation can be established at the 3σ level if the error ellipses do not overlap the CP-conserving curves (solid lines, $\delta=0$). The curves for the other CP-conserving case ($\delta=180°$) lie very close to the $\delta=0$ curves and are not shown.

Note that for scenario W with the upgraded 4 MW SJHF beam, if $\sin^2 2\theta_{13}=0.1$ (larger values are already excluded), $\delta m_{21}^2=5\times10^{-5}$ eV^2, and $\delta=90°$, then the predicted point in the $[N(e-),N(e+)]$ plane is just 3σ away from the CP conserving $[N(e+)=N(e-)]$ prediction. Alternatively, if $\sin^2 2\theta_{13}=0.02$, $\delta m_{21}^2=1\times10^{-4}$ eV^2 (larger values are improbable), and $\delta=90°$, then the predicted point is also just

3σ away from the CP-conserving prediction. Hence there is a small region of the allowed parameter space ($\sin^2 2\theta_{13} >0.02$ and $\delta m_{21}^2>5\times10^{-5}$ eV^2) within which maximal CP violation might be observable at an upgraded JHF if δm_{32}^2 is in the center of the presently favored SuperK region and $\sin^2 2\theta_{23}\sim1$. It is also possible to detect maximal CP violation for $\sin^2 2\theta_{13}>0.05$ and $\delta m_{21}^2>10^{-4}$ eV^2 with the 0.77 MW JHF in the W scenario. Generally detector scenario W does better for CP violation, except scenario A is slightly better for $\sin^2 2\theta_{13}\simeq0.02$ at the 4 MW SJHF. Because the matter effect is small at $L=295$ km, predictions for $\delta m_{32}^2 >0$ and $\delta m_{32}^2<0$ are nearly the same, and hence the sign of δm_{32}^2 cannot be determined.

B. CP violation and the sign of δm_{32}^2 at long-baseline experiments

Consider next long-baseline experiments using multi-GeV neutrino beams. The approximate equality $N(e+)\simeq N(e-)$ will be modified by intrinsic CP violation and by matter effects. Predictions in the $[N(e-),N(e+)]$ plane are shown in Fig. 9 for scenario A using the 1.6 MW LE superbeam for two values of δm_{21}^2 (5×10^{-5} eV^2 and 1×10^{-4}
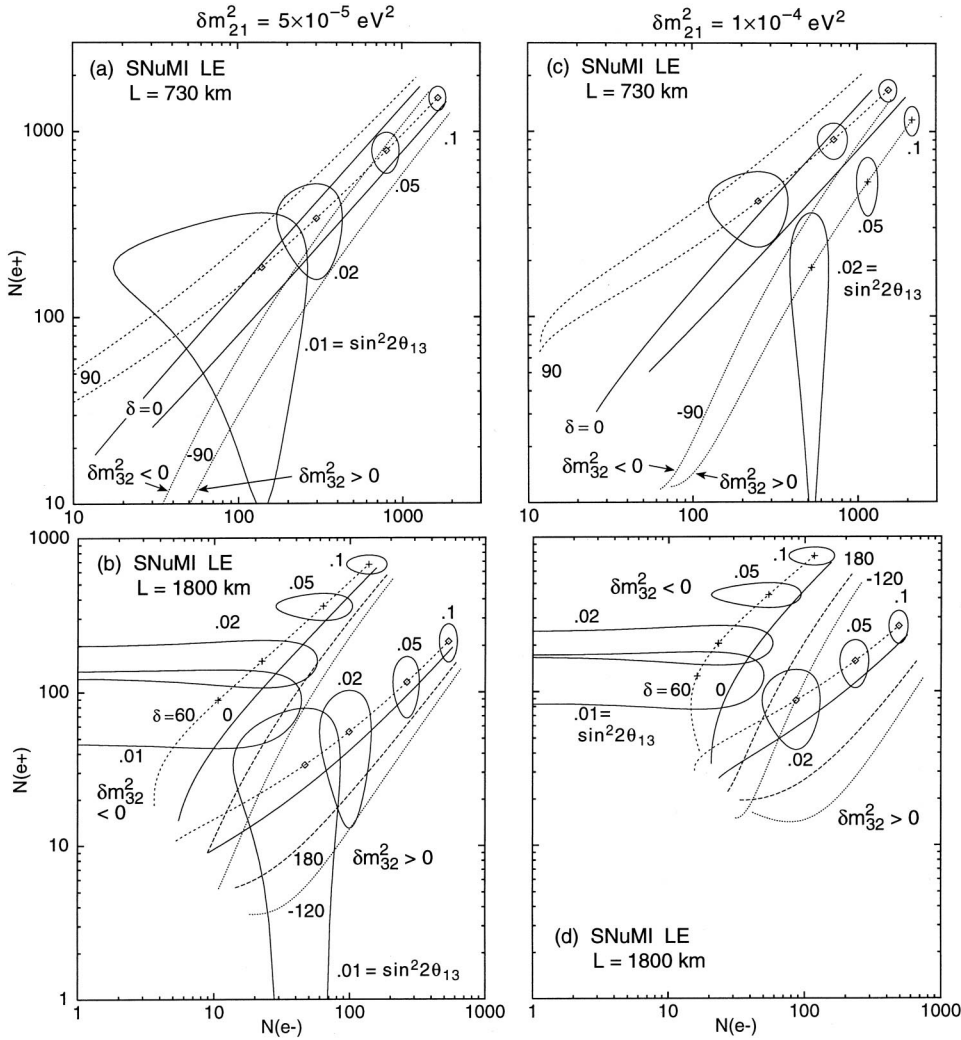
FIG. 9. 3σ error ellipses in the $[N(e^+), N(e^-)]$ plane, shown for detector scenario A at the upgraded LE SNuMI beam with $L = 730$ (top plots) and 1800 km (bottom plots). The contours are shown for $\delta m_{21}^2 = 5 \times 10^{-5}$ (left) and 10^{-4} eV^2 (right). The solid and long-dashed curves correspond to the CP conserving cases $\delta = 0°$ and $180°$, and the short-dashed and dotted curves correspond to two other cases that give the largest deviation from the CP conserving curves; along these curves $\sin^2 2\theta_{13}$ varies from 0.001 to 0.1, as indicated.

eV^2) and for two baselines ($L = 730$ km and 1800 km). The predictions for each of these cases are shown as a function of $\sin^2 2\theta_{13}$, δ, and the sign of δm_{32}^2, with $|\delta m_{32}^2| = 3.5 \times 10^{-3}$ eV^2 and $\sin^2 2\theta_{23} = 1$. Note that at $L = 730$ km the magnitude of the modifications of the appearance rates due to matter effects are comparable to the magnitudes of the modifications due to maximal intrinsic CP violation. Furthermore, the expected precisions of the measurements, shown on the figure by the 3σ error ellipses, are also comparable to the sizes of the predicted CP and matter effects.

Matter effects will cause the two CP-conserving cases $\delta = 0$ and $\delta = 180°$ to give different predictions for $N(e^+)$ and $N(e^-)$, and therefore to establish CP violation the signal must be distinguishable from both $\delta = 0$ and $\delta = 180°$. Hence, in the scenario we are considering, Fig. 9 shows that superbeam measurements with the LE beam at 730 km can help to constrain the parameter space, but generally cannot provide unambiguous evidence for intrinsic CP violation and cannot unambiguously determine the sign of δm_{32}^2. The only exception to this is if $\delta m_{32}^2 > 0$ and $\delta = -90°$ (or $\delta m_{32}^2 < 0$ and $\delta = 90°$), in which case CP violation could be established and the sign of δm_{32}^2 determined for $\sin^2 2\theta_{13}$

> 0.02. The CP and matter effects are better separated at $L = 1800$ km, for which an unambiguous determination of the sign of δm_{32}^2 seems possible provided $\sin^2 2\theta_{13} > 0.02$, although CP violation cannot be established for $\delta m_{21}^2 < 10^{-4}$ eV^2. At smaller values of $\sin^2 2\theta_{13}$ modifications to the appearance rates cannot distinguish between matter and CP effects. Note that, because of the matter effect, at distances longer than 1000 km the values of δ that give the largest disparity of $N(e^+)$ and $N(e^-)$ are no longer $\pm 90°$. Also note that the sign of δm_{32}^2 is most easily determined when the CPV and matter effects interfere constructively to give a greater disparity of $N(e^+)$ and $N(e^-)$, and more difficult when the CPV and matter effects interfere destructively [i.e., $N(e^+)$ and $N(e^-)$ are more equal]. Going to even longer baselines, predictions in the $[N(e-), N(e+)]$ plane are shown in Fig. 10 for scenario A (left-hand plots) and scenario W (right-hand plots) with $L = 2900$ km. The predictions are shown for the LE beam (top plots), ME beam (middle plots), and HE beam (bottom plots). In general, the sign of δm_{32}^2 can be determined provided $\sin^2 2\theta_{13} > 0.02$, but in none of the explored long-baseline scenarios can CP violation be unambiguously established for $\delta m_{21}^2 < 10^{-4}$ eV^2.
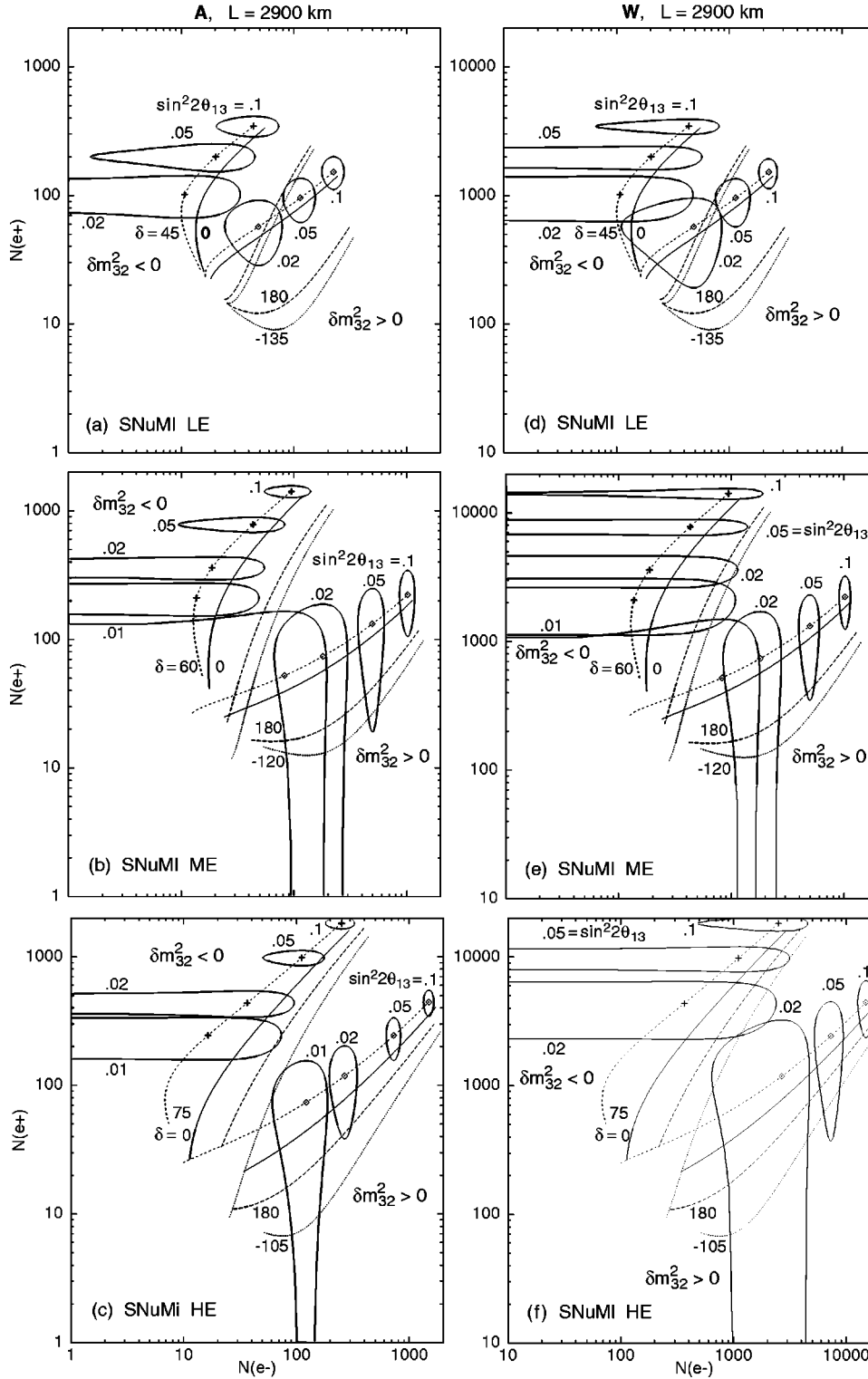
FIG. 10. 3σ error ellipses in the $[N(e^+),N(e^-)]$ plane, shown for detector scenarios A (left) and W (right) at $L=2900$ km with the upgraded LE (top), ME (center), and HE (bottom) SNuMI beams. The contours are shown for $\delta m_{21}^2 = 10^{-4}$ eV^2. The solid and long-dashed curves correspond to the CP conserving cases $\delta = 0°$ and $180°$, and the short-dashed and dotted curves correspond to two other cases that give the largest deviation from the CP conserving curves; along these curves $\sin^2 2\theta_{13}$ varies from 0.001 to 0.1, as indicated.

C. *CP* violation and the sign of δm_{32}^2 at a neutrino factory

We can ask, how do the CPV and δm_{32}^2 sign capabilities of superbeams compare with those of a neutrino factory? The relevant experimental signature at neutrino factory is the appearance of a wrong-sign muon, indicating $\nu_e \rightarrow \nu_\mu$ (or $\bar{\nu}_e \rightarrow \bar{\nu}_\mu$) transitions. This is a much cleaner signature than electron appearance with a superbeam. Hence, background systematics are under better control at a neutrino factory, and the expected error ellipses in the $[N(\mu+), N(\mu-)]$ plane are therefore much smaller.

In our analysis we assume a 20 GeV neutrino factory with 1.8×10^{21} useful μ^+ decays (which might be achieved in three years running at at high-performance neutrino factory) and 3.6×10^{21} useful μ^- decays, a 50 kt iron-scintillator detector [49] at distances $L=1800$ km, 2900 km, and 4000 km
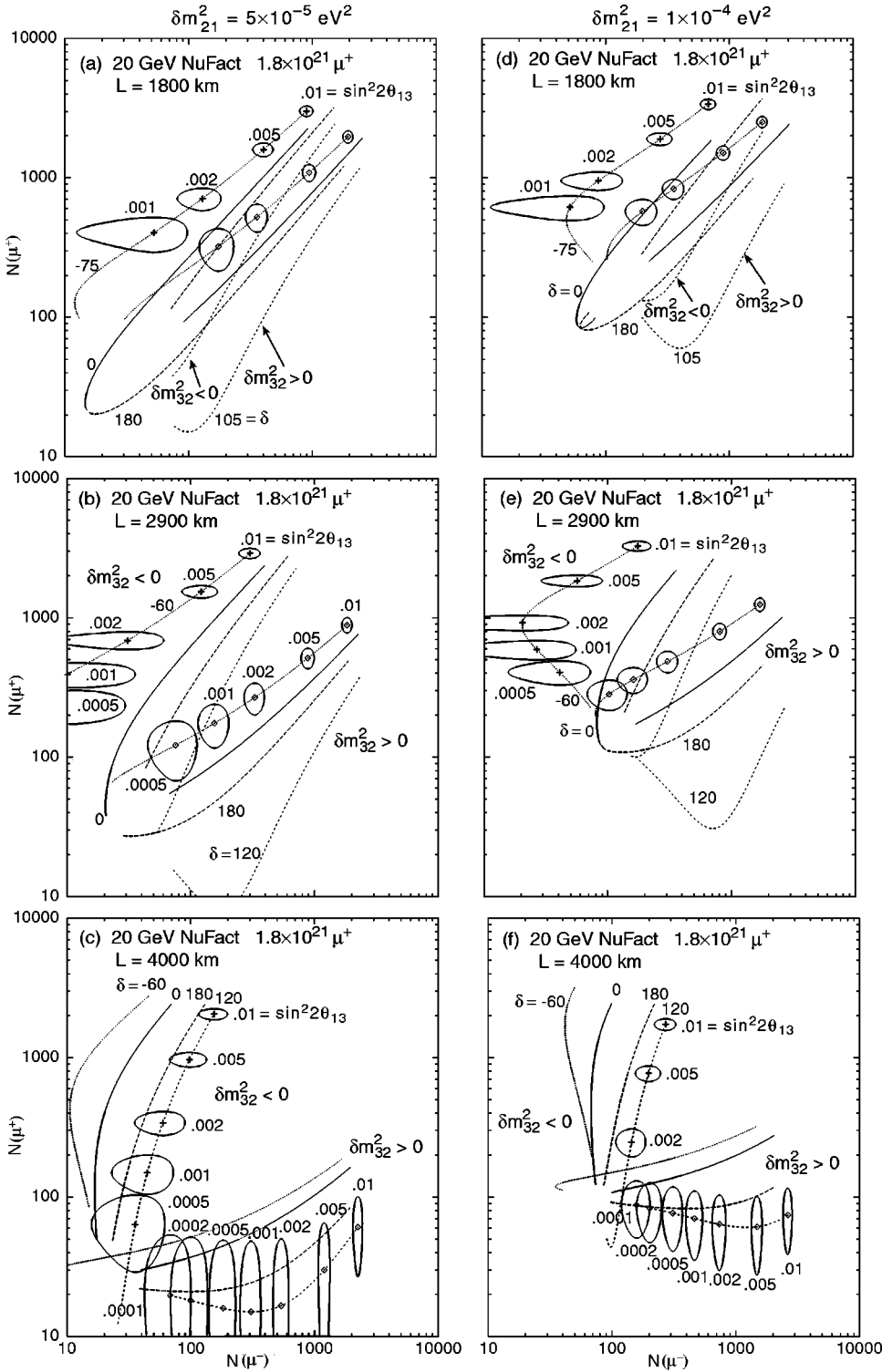
FIG. 11. 3σ error ellipses in the $[N(\mu^+),N(\mu^-)]$ plane, shown for a neutrino factory delivering 3.6×10^{21} useful decays of 20 GeV muons and 1.8×10^{21} useful decays of 20 GeV anti-muons, with a 50 kt detector at $L=1800$ (top), 2900 (center), and 4000 km (bottom), with $\delta m_{21}^2=5\times10^{-5}$ (left) and 10^{-4} eV^2 (right). The solid and long-dashed curves correspond to the CP conserving cases $\delta=0°$ and $180°$, and the short-dashed and dotted curves correspond to two other cases that give the largest deviation from the CP conserving curves; along these curves $\sin^2 2\theta_{13}$ varies from 0.0001 to 0.01, as indicated.

from the source. For comparison, the total neutrino flux for three years running at a distance of 1 km from the source is $2\times10^{19}/\text{m}^2$ for the neutrino factory scenario, while it is $7\times10^{16}/\text{m}^2$ for SJHF and $4\times10^{18}/\text{m}^2$ for the SNuMI HE beam. We choose an iron-scintillator detector for the neutrino factory analysis since it is particularly well suited for the detection of muons and can be made larger than, e.g., a liquid argon detector, at a similar or lower cost. We also take $f_B=10^{-4}$, $\sigma_{f_B}/f_B=0.1$, and a normalization uncertainty of

2%. This background level can be achieved with a 4 GeV cut on the detected muon, which gives a detection efficiency of about 73%, implying an effective data sample of $D=110$ kt yr for three years running.

The corresponding neutrino factory predictions in the $[N(\mu-), N(\mu+)]$ plane are shown in Fig. 11. The 1800 km baseline is too short, since matter and CP effects are indistinguishable in most cases. At 2900 km the predictions allow an unambiguous determination of the sign of δm_{32}^2 for much
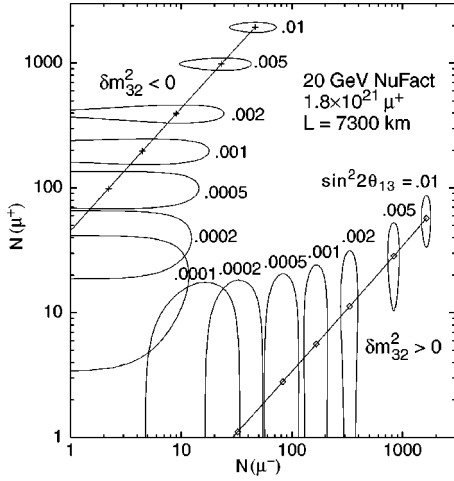
FIG. 12. 3σ error ellipses in the $[N(\mu^+),N(\mu^-)]$ plane, shown for a neutrino factory delivering 3.6×10^{21} useful decays of 20 GeV muons and 1.8×10^{21} useful decays of 20 GeV antimuons, with a 50 kt detector at $L=7300$ km, $\delta m^2_{21}=10^{-4}$ eV^2, and $\delta=0$. Curves are shown for both signs of δm^2_{32}; $\sin^2 2\theta_{13}$ varies along the curves from 0.0001 to 0.01, as indicated.

of the parameter space, and the possibility of establishing the existence of CPV. At 4000 km the statistical uncertainties are larger, and impair the sensitivity to observe CPV. However, matter effects are also larger, and an unambiguous determination of the sign of δm^2_{32} is possible down to $\sin^2 2\theta_{13}$ of a few $\times 10^{-4}$. For very long baselines (e.g. $L=7300$ km, Fig. 12) there is negligible sensitivity to CPV or to δm^2_{21}, matter effects are large, and the $\sin^2 2\theta_{13}$ reach for determining the sign of δm^2_{32} approaches 10^{-4}.

VI. SUMMARY

We have explored the oscillation-physics capabilities of 1 GeV and multi-GeV neutrino beams produced at MW-scale proton accelerator facilities (neutrino superbeams). Specifically, the limiting value of $\sin^2 2\theta_{13}$ that would permit the first observation of $\nu_\mu \to \nu_e$ and/or $\bar\nu_\mu \to \bar\nu_e$ oscillations at 3 standard deviations is considered, along with the ability of these intense conventional neutrino beams to determine the pattern of neutrino masses (sign of δm^2_{32}) and discover CP violation in the lepton sector. The figures in this paper provide a toolkit for accessing the physics capabilities as a function of the detector specifications, characterized by the data set size D (kt yr) and the uncertainty on the background subtraction (given by f_B and σ_{f_B}/f_B). Table V summarizes the physics capabilities of some beam-detector combinations. Also shown in the table are similar results for an entry-level and high-performance neutrino factory with $E_\mu = 20$ GeV.

Determining the optimum detector technology and characteristics is beyond the scope of this paper, and may require a detector research and development program. However, for some ambitious but plausible detector scenarios we find the following:

(i) With a sufficiently ambitious detector, if $\sin^2 2\theta_{13} >$ few $\times 10^{-3}$ and $\delta m^2_{32}>0$, then $\nu_\mu \to \nu_e$ and $\bar\nu_\mu \to \bar\nu_e$ signals

should be observable at a superbeam. The reach is slightly worse if $\delta m^2_{32}<0$. The best reach is obtained with a long-baseline multi-GeV superbeam; for example, with the SNuMI ME or HE beams and a baseline $\geqslant 2000$ km. This would permit the tightening of constraints on the oscillation parameter space. It is important to account for decay channel length restrictions when assessing the capabilities of very-long-baseline experiments.

(ii) If CP is maximally violated in the lepton sector, there is a small region of allowed parameter space in which an experiment at a JHF or SJHF beam ($E_\nu \sim 1$ GeV) might be able to establish CP violation at 3 standard deviations. Except for certain small regions in parameter space where matter and CPV effects constructively interfere, a long-baseline experiment with conventional superbeams would be unable to unambiguously establish CP violation because matter effects can confuse the interpretation of the measurements.

(iii) With a sufficiently ambitious detector, if $\sin^2 2\theta_{13} > \mathcal{O}(0.01)$, there is a significant region of parameter space over which a long-baseline experiment with a multi-GeV neutrino superbeam could unambiguously establish the sign of δm^2_{32}.

(iv) Lower-energy superbeams do best at shorter distances, with a fair reach for $\nu_\mu \to \nu_e$ appearance and some CPV capability, but little or no sensitivity to the sign of δm^2_{32}; higher-energy superbeams do best at longer distances, with good reach for $\nu_\mu \to \nu_e$ appearance and sgn(δm^2_{32}) determination, but little or no sensitivity to CPV.

(v) A neutrino factory can deliver between one and two orders of magnitude better reach in $\sin^2 2\theta_{13}$ for $\nu_e \to \nu_\mu$ appearance, the sign of δm^2_{32}, and CP violation; for $L \sim 3000$ km there is excellent sensitivity to all three observables.

Note that in this study we have restricted our considerations to 1 GeV and multi-GeV neutrino beams. The potential of sub-GeV beams is currently under consideration [77,78].

APPENDIX

To implement the Poisson statistical uncertainties in our analysis of the $\sin^2 2\theta_{13}$ reach we use an approximate expression for the upper limit (λ_U) on the number of events from the observation of N events,

$$\lambda_U \simeq N + S\sqrt{N+1} + (S^2+2)/3, \qquad (A1)$$

where S is the number of standard deviations corresponding to the limit. This expression gives the correct λ_U with an accuracy that is better than 10% for $N<4$ and better than 1% for larger N [79]. If the number of predicted background

TABLE V. Summary of the $\sin^2 2\theta_{13}$ reach (in units of 10^{-3}) for various combinations of neutrino beam, distance, and detector for (i) a 3σ $\nu_\mu \to \nu_e$ appearance with $\delta m_{21}^2 = 10^{-5}$ eV^2, (ii) a 3σ determination of the sign of δm_{32}^2 with $\delta m_{21}^2 = 5 \times 10^{-5}$ eV^2 , and (iii) a 3σ discovery of CP violation for three values of δm_{21}^2 (in eV^2). Dashes in the sign of δm_{32}^2 column indicate that the sign is not always determinable. Dashes in the CPV columns indicate CPV cannot be established for $\sin^2 2\theta_{13} \lesssim 0.1$, the current experimental upper limit, for any values of the other parameters. The CPV entries are calculated assuming the value of δ that gives the maximal disparity of $N(e^+)$ and $N(e^-)$; for other values of δ, CP violation may not be measurable.

| | | | $\sin^2 2\theta_{13}$ reach (in units of 10^{-3}) | | | | |
| | | | $\nu_\mu \to \nu_e$ appearance | Unambiguous 3σ sign(δm_{32}^2) | Possible 3σ CPV δm_{21}^2 (in eV^2) | | |
Beam	L (km)	Detector	$\delta m_{21}^2 = 10^{-5}$	$\delta m_{21}^2 = 5 \times 10^{-5}$	5×10^{-5}	1×10^{-4}	2×10^{-4}
JHF	295	A	25	−	−	−	25
		W	17	−	−	40	8
SJHF	295	A	8	−	−	5	3
		W	15	−	100	20	5
SNuMI LE	730	A	7	−	100	20	4
		W	30	−	−	−	40
SNuMI ME	2900	A	3	6	−	−	100
		W	8	15	−	−	−
	7300	A	6	6	−	−	−
		W	3	3	−	−	−
SNuMI HE	2900	A	3	7	−	100	20
		W	10	15	−	−	−
	7300	A	4	4	−	−	−
		W	3	3	−	−	−
20 GeV NuF 1.8×10^{20} μ^+	2900	50 kt	0.5	2.5	−	2	1.5
	7300		0.5	0.3	−	−	−
20 GeV NuF 1.8×10^{21} μ^+	2900	50 kt	0.1	1.2	0.6	0.4	0.6
	7300		0.07	0.1	−	−	−

events is B, the expected number of signal events corresponding to an observation 3 statistical standard deviations above the background is given by

$$N_s = 3\sqrt{B+1} + 11/3. \tag{A2}$$

Let the systematic uncertainty on B be given by U. To account for this systematic uncertainty, we add it in quadrature with the statistical uncertainty. Defining the quantity

$$N_s' = \sqrt{N_s^2 + 9U^2}, \tag{A3}$$

the $\sin^2 2\theta_{13}$ reach can then be estimated by finding the value of $\sin^2 2\theta_{13}$ that yields N_s' signal events.

To determine the sign of δm_{32}^2 and/or search for CP violation with conventional ν_μ and $\bar{\nu}_\mu$ beams, we will need to compare the $\nu_\mu \to \nu_e$ and $\bar{\nu}_\mu \to \bar{\nu}_e$ appearance rates (for a neutrino factory with a detector that measures muons, we compare the $\nu_e \to \nu_\mu$ and $\bar{\nu}_e \to \bar{\nu}_\mu$ appearance rates). As in the case of the $\sin^2 2\theta_{13}$ reach, we will be considering the 3σ allowed regions.

Let N and $\bar{N}$ be the number of events that satisfy the signal selection criteria and are recorded respectively during neutrino and antineutrino running. If N^{th} and $\bar{N}^{th}$ are theoretical predictions for N and $\bar{N}$, the region of the Nth-$\bar{N}^{th}$ space allowed by the measurements is described by

$$\left(\frac{N^{th}-N}{\alpha_N}\right)^2 + \left(\frac{\bar{N}^{th}-\bar{N}}{\alpha_{\bar{N}}}\right)^2 \leq 1, \tag{A4}$$

where α_N and $\alpha_{\bar{N}}$ are the experimental uncertainties on N and $\bar{N}$, respectively. In the absence of systematic uncertainties and in the approximation of Gaussian statistics, the 3σ values are $\alpha_N = 3\sqrt{N}$ and $\alpha_{\bar{N}} = 3\sqrt{\bar{N}}$. However, since N and $\bar{N}$ might be small Gaussian statistics may be inappropriate. Instead, we define α_N and $\alpha_{\bar{N}}$ to correspond to the appropriate 99.87% confidence level deviations from the central values of N and $\bar{N}$, respectively, using Poisson statistics. The expressions for α_N and $\alpha_{\bar{N}}$ will depend on whether we are considering an upper or lower limit.

Consider first the case of an upper limit. We can compute α_N using Eq. (A1), with $S=3$, yielding

$$\alpha_N^{upper} = 3\sqrt{N+1} + 11/3. \tag{A5}$$

To compute the value for $\alpha_{\bar{N}}$ for a lower bound, we need an expression for the Poisson lower limit given the observation of N events. We use the expression from Ref. [79], namely,

$$\lambda_L \simeq N\left(1 - \frac{1}{9N} - \frac{S}{3\sqrt{N}} + \beta N^\gamma\right)^3, \tag{A6}$$

where with $S=3$ we have $\beta = 0.222$ and $\gamma = -1.88$. This approximate expression for the Poisson lower limit on N is accurate to a few percent or better for all N. Hence

$$\alpha_N^{lower} = N - N\left(1 - \frac{1}{9N} - \frac{3}{3\sqrt{N}} + 0.222 N^{-1.88}\right)^3. \tag{A7}$$

The corresponding values for $\alpha_{\bar{N}}$ can be found by substituting $\bar{N}$ for N in Eqs. (A5) and (A7).

In practice N and $\bar{N}$ will contain background components B and $\bar{B}$. The predicted backgrounds will have associated systematic uncertainties U and $\bar{U}$. In this case we can still use Eq. (A4) to determine the allowed regions, but to take account of the background and systematic uncertainties the α_N^2 and $\alpha_{\bar{N}}^2$ are replaced with the substitutions

$$\alpha_N^2 \rightarrow \alpha_N^2 + 9U^2 \tag{A8}$$

$$\alpha_{\bar{N}}^2 \rightarrow \alpha_{\bar{N}}^2 + 9\bar{U}^2. \tag{A9}$$

Other systematic uncertainties on the predicted N and $\bar{N}$ (for example, the uncertainty on the neutrino and antineutrino cross sections) can be handled in a similar way, by replacing α_N ($\alpha_{\bar{N}}$) with the quadrature sum of α_N ($\alpha_{\bar{N}}$) and the additional 99.87% C.L. uncertainty in N ($\bar{N}$).

---

[1] Super-Kamiokande Collaboration, Y. Fukuda *et al.*, Phys. Lett. B **433**, 9 (1998); **436**, 33 (1998); Phys. Rev. Lett. **81**, 1562 (1998); **82**, 2644 (1999).

[2] Kamiokande Collaboration, K.S. Hirata *et al.*, Phys. Lett. B **280**, 146 (1992); Y. Fukuda *et al.*, *ibid.* **335**, 237 (1994); IMB Collaboration, R. Becker-Szendy *et al.*, Nucl. Phys. B (Proc. Suppl.) **38**, 331 (1995); Soudan-2 Collaboration, W.W.M. Allison *et al.*, Phys. Lett. B **391**, 491 (1997); MACRO Collaboration, M. Ambrosio *et al.*, *ibid.* **434**, 451 (1998).

[3] G. Barr, T.K. Gaisser, and T. Stanev, Phys. Rev. D **39**, 3532 (1989); M. Honda, T. Kajita, K. Kasahara, and S. Midorikawa, *ibid.* **52**, 4985 (1995); V. Agrawal, T.K. Gaisser, P. Lipari, and T. Stanev, *ibid.* **53**, 1314 (1996); T.K. Gaisser *et al.*, *ibid.* **54**, 5578 (1996); T.K. Gaisser and T. Stanev, *ibid.* **57**, 1977 (1998); P. Lipari, Astropart. Phys. **14**, 153 (2000).

[4] V. Barger and K. Whisnant, Phys. Lett. B **209**, 365 (1988); J.G. Learned, S. Pakvasa, and T.J. Weiler, *ibid.* **207**, 79 (1988); K. Hidaka, M. Honda, and S. Midorikawa, Phys. Rev. Lett. **61**, 1537 (1988).

[5] S.M. Bilenky, C. Giunti, and W. Grimus, Eur. Phys. J. C **1**, 247 (1998); V. Barger, K. Whisnant, and T.J. Weiler, Phys. Lett. B **427**, 97 (1998); V. Barger, S. Pakvasa, T.J. Weiler, and K. Whisnant, Phys. Rev. D **58**, 093016 (1998); V. Barger, Yuan-Ben Dai, K. Whisnant, and B.-L. Young, *ibid.* **59**, 113010 (1999); O. Yasuda, talk given at 30th International Conference on High-Energy Physics (ICHEP 2000), Osaka, Japan, 2000, hep-ph/0008256; T. Hattori, T. Hasuike, and S. Wakaizumi, hep-ph/0010232. Additional references can be found in V. Barger and K. Whisnant, in *Current Aspects of Neutrino Physics*, edited by D. Caldwell (Springer-Verlag, Hamburg, in press), hep-ph/0006235.

[6] CHOOZ Collaboration, M. Apollonio *et al.*, Phys. Lett. B **420**, 320 (1998); Palo Verde Collaboration, C. Gratta, talk at *Neutrino-2000*, XIXth International Conference on Neutrino Physics and Astrophysics, Sudbury, Canada, 2000.

[7] L. Wolfenstein, Phys. Rev. D **17**, 2369 (1978); V. Barger, S. Pakvasa, R.J.N. Phillips, and K. Whisnant, *ibid.* **22**, 2718 (1980).

[8] V. Barger, N. Deshpande, P.B. Pal, R.J.N. Phillips, and K. Whisnant, Phys. Rev. D **43**, R1759 (1991).

[9] T. Toshita, talk given at 30th International Conference on High-Energy Physics (ICHEP 2000), Osaka, Japan, 2000.

[10] G.L. Fogli, E. Lisi, and A. Marrone, Phys. Rev. D **63**, 053008 (2001).

[11] V. Barger, J.G. Learned, S. Pakvasa, and T.J. Weiler, Phys. Rev. Lett. **82**, 2640 (1999); V. Barger, J.G. Learned, P. Lipari, M. Lusignoli, S. Pakvasa, and T.J. Weiler, Phys. Lett. B **462**, 109 (1999).

[12] A. Acker, A. Joshipura, and S. Pakvasa, Phys. Lett. B **285**, 371 (1992); G. Gelmini and J.W.F. Valle, Phys. Lett. **142B**, 181 (1984); K. Choi and A. Santamaria, Phys. Lett. B **267**, 504 (1991); A.S. Joshipura, PRL Report-PRL-TH-91/6; A.S. Joshipura and S. Rindani, Phys. Rev. D **46**, 3000 (1992).

[13] KEK-PS E362 Collaboration, K. Nishikawa *et al.*, ''Proposal for a Long Baseline Neutrino Oscillation Experiment, using KEK-PS and Super-Kamiokande,'' 1995 (unpublished); talk presented by K2K Collaboration, M. Sakuda, at the XXXth International Conference on High Energy Physics (ICHEP 2000), Osaka, Japan, 2000.

[14] MINOS Collaboration, ''Neutrino Oscillation Physics at Fermilab: The NuMI-MINOS Project,'' Report No. NuMI-L-375, 1998.

[15] See the ICARUS/ICANOE web page at http://pcnometh4.cern.ch/

[16] See the OPERA web page at http://www.cern.ch/opera/

[17] B.T. Cleveland *et al.*, Nucl. Phys. B (Proc. Suppl.) **38**, 47 (1995).

[18] Kamiokande Collaboration, Y. Fukuda *et al.*, Phys. Rev. Lett. **77**, 1683 (1996).

[19] Super-Kamiokande Collaboration, Y. Fukuda *et al.*, Phys. Rev. Lett. **81**, 1158 (1998); **82**, 1810 (1999); **82**, 2430 (1999).

[20] GALLEX Collaboration, W. Hampel *et al.*, Phys. Lett. B **388**,

384 (1996); SAGE Collaboration, J.N. Abdurashitov *et al.*, Phys. Rev. Lett. **77**, 4708 (1996); GNO Collaboration, M. Altmann *et al.*, Phys. Lett. B **490**, 16 (2000).

[21] J.N. Bahcall and M.H. Pinsonneault, Rev. Mod. Phys. **67**, 781 (1995); J.N. Bahcall, S. Basu, and M.H. Pinsonneault, Phys. Lett. B **433**, 1 (1998).

[22] N. Hata and P. Langacker, Phys. Rev. D **56**, 6107 (1997); J.N. Bahcall, M.H. Pinsonneault, and S. Basu, Astrophys. J. (to be published), astro-ph/0010346.

[23] Y. Takeuchi, talk given at 30th International Conference on High-Energy Physics (ICHEP 2000), Osaka, Japan, 2000.

[24] S.P. Mikheyev and A. Smirnov, Yad. Fiz. **42**, 1441 (1985) [Sov. J. Nucl. Phys. **42**, 913 (1986)]; P. Langacker, J.P. Leveille, and J. Sheiman, Phys. Rev. D **27**, 1228 (1983).

[25] G. Fogli, E. Lisi, D. Montanino, and A. Palazzo, Phys. Rev. D **62**, 113003 (2000); M.C. Gonzalez-Garcia, C. Pena-Garay, Y. Nir, and A. Yu. Smirnov, *ibid.* **63**, 013007 (2001); J.N. Bahcall, P.I. Krastev, A.Yu. Smirnov, *ibid.* **60**, 093001 (1999); J.N. Bahcall and P.I. Krastev, Phys. Rev. C **56**, 2839 (1997); M. Maris and S. Petcov, Phys. Rev. D **58**, 113008 (1998); **56**, 7444 (1997); hep-ph/0004151; Q.Y. Liu, M. Maris, and S. Petcov, Phys. Rev. D **56**, 5991 (1997); E. Lisi and D. Montanino, *ibid.* **56**, 1792 (1997); A.H. Guth, L. Randall, and M. Serna, J. High Energy Phys. **08**, 019 (1999); A. de Gouvea, A. Friedland, and H. Murayama, *ibid.* **03**, 009 (2001).

[26] M.C. Gonzales-Garcia and C. Pena-Garay, Nucl. Phys. B (Proc. Suppl.) **91**, 80 (2000); M.C. Gonzalez-Garcia, M. Maltoni, C. Pena-Garay, and J.W.F. Valle, Phys. Rev. D **63**, 033005 (2001); R. Barbieri and A. Strumia, J. High Energy Phys. **12**, 016 (2000).

[27] V. Barger, B. Kayser, J.G. Learned, T.J. Weiler, and K. Whisnant, Phys. Lett. B **489**, 345 (2000).

[28] O.L.G. Peres and A.Yu. Smirnov, Nucl. Phys. **B599**, 3 (2001).

[29] KamLAND proposal, Stanford-HEP-98-03; A. Piepke, talk at ''Neutrino-2000,'' XIXth International Conference on Neutrino Physics and Astrophysics, Sudbury, Canada, 2000.

[30] V. Barger, D. Marfatia, and B.W. Wood, Phys. Lett. B **498**, 53 (2001).

[31] LSND Collaboration, C. Athanassopoulos *et al.*, Phys. Rev. Lett. **77**, 3082 (1996); **81**, 1774 (1998); G. Mills, talk at ''Neutrino-2000'' [29].

[32] A. Bazarko, MiniBooNE Collaboration, talk at ''Neutrino-2000'' [29].

[33] B. Richter, hep-ph/0008222.

[34] K. Dick, M. Freund, P. Huber, and M. Lindner, Nucl. Phys. **B598**, 543 (2001).

[35] S. Geer, Phys. Rev. D **57**, 6989 (1998).

[36] V. Barger, S. Geer, and K. Whisnant, Phys. Rev. D **61**, 053004 (2000).

[37] V. Barger, S. Geer, R. Raja, and K. Whisnant, Phys. Rev. D **63**, 033002 (2001).

[38] V. Barger, S. Geer, R. Raja, and K. Whisnant, Phys. Lett. B **485**, 379 (2000).

[39] H.W. Zaglauer and K.H. Schwarzer, Z. Phys. C **40**, 273 (1988).

[40] R.H. Bernstein and S.J. Parke, Phys. Rev. D **44**, 2069 (1991).

[41] V. Barger, S. Geer, R. Raja, and K. Whisnant, Phys. Rev. D **62**, 013004 (2000).

[42] V. Barger, S. Geer, R. Raja, and K. Whisnant, Phys. Rev. D **62**, 073002 (2000).

[43] P. Lipari, Phys. Rev. D **61**, 113004 (2000).

[44] A. De Rujula, M.B. Gavela, and P. Hernandez, Nucl. Phys. **B547**, 21 (1999).

[45] A. Donini, M.B. Gavela, P. Hernandez, and S. Rigolin, Nucl. Phys. **B574**, 23 (2000); A. Cervera, A. Donini, M.B. Gavela, J.J. Gomez Cadenas, P. Hernandez, O. Mena, and S. Rigolin, Nucl. Phys. **B579**, 17 (2000); **B593**, 731(E) (2001).

[46] K. Dick, M. Freund, M. Lindner, and A. Romanino, Nucl. Phys. **B562**, 299 (1999); A. Romanino, *ibid.* **B574**, 675 (2000); M. Freund, M. Lindner, S.T. Petcov, and A. Romanino, *ibid.* **B578**, 27 (2000).

[47] M. Freund, P. Huber, and M. Lindner, Nucl. Phys. **B585**, 105 (2000).

[48] K.T. McDonald *et al.*, Neutrino Factory and Muon Collider Collaboration, physics/9911009.

[49] C. Albright *et al.*, hep-ex/0008064.

[50] M. Campanelli, A. Bueno, and A. Rubbia, hep-ph/9905240; A. Bueno, M. Campanelli, and A. Rubbia, Nucl. Phys. **B573**, 27 (2000); **B589**, 577 (2000).

[51] M. Koike and J. Sato, Phys. Rev. D **61**, 073012 (2000).

[52] O. Yasuda, hep-ph/0005134.

[53] P.F. Harrison and W.G. Scott, Phys. Lett. B **476**, 349 (2000); H. Yokomakura, K. Kimura, and A. Takamura, *ibid.* **496**, 175 (2000); S.J. Parke and T.J. Weiler, *ibid.* **501**, 106 (2001); Z.Z. Xing, *ibid.* **487**, 327 (2000); Phys. Rev. D **63**, 073012 (2001).

[54] J. Arafune and J. Sato, Phys. Rev. D **55**, 1653 (1997); M. Koike and J. Sato, hep-ph/9707203; J. Arafune, M. Koike, and J. Sato, Phys. Rev. D **56**, 3093 (1997); T. Ota and J. Sato, *ibid.* **63**, 093004 (2001).

[55] T. Hattori, T. Hasuike, and S. Wakaizumi, Phys. Rev. D **62**, 033006 (2000).

[56] V. Barger, R.J.N. Phillips, and K. Whisnant, Phys. Rev. Lett. **45**, 2084 (1980).

[57] S. Pakvasa, in *High Energy Physics—1980*, edited by L. Durand and L.G. Pondrom, AIP Conf. Proc. No. 68 (AIP, New York, 1981), p. 1164.

[58] T.K. Kuo and J. Pantaleone, Rev. Mod. Phys. **61**, 937 (1989).

[59] Parameters of the Preliminary Reference Earth Model are given by A. Dziewonski, Earth Structure, Global, in *The Encyclopedia of Solid Earth Geophysics*, edited by by D.E. James (Van Nostrand Reinhold, New York, 1989), p. 331; also see R. Gandhi, C. Quigg, M. Hall Reno, and I. Sarcevic, Astropart. Phys. **5**, 81 (1996).

[60] W.-Y. Keung and L.-L. Chau, Phys. Rev. Lett. **53**, 1802 (1984).

[61] C. Jarlskog, Z. Phys. C **29**, 491 (1985); Phys. Rev. D **35**, 1685 (1987).

[62] S. Coleman and S.L. Glashow, Phys. Rev. D **59**, 116008 (1999).

[63] V. Barger, S. Pakvasa, T.J. Weiler, and K. Whisnant, Phys. Rev. Lett. **85**, 5055 (2000).

[64] H. Murayama and T. Yanagida, hep-ph/0010178.

[65] Talk presented by W. Marciano at the Joint U.S./Japan Workshop on New Initiatives in Muon Lepton Flavor Violation and Neutrino Oscillation with High Intense Muon and Neutrino Sources, Honolulu, Hawaii, 2000, http://meco.ps.uci.edu/lepton_workshop/talks/marciano.pdf

[66] I. Mocioiu and R. Shrock, in *Next Generation Nucleon Decay*

and Neutrino Detector, edited by M.V. Diwan and C.K. Jung, AIP Conf. Proc. No. 533 (AIP, Melville, NY, 2000), p. 74; Phys. Rev. D **62**, 053017 (2000).

[67] J. Pantaleone, Phys. Rev. Lett. **81**, 5060 (1998).

[68] JHF LOI, http://www-jhf.kek.jp/

[69] See also talks by D. Casper, K. Nakamura, Y. Obayashi, and Y.F. Wang at the Joint U.S./Japan Workshop on New Initiatives in Muon Lepton Flavor Violation and Neutrino Oscillation with High Intense Muon and Neutrino Sources, Honolulu, Hawaii, 2000, http://meco.ps.uci.edu/lepton_workshop/talks/

[70] M. Aoki (private communication).

[71] W. Chou, FERMILAB-Conf-97/199, Proc. 1997 Particle Accel. Conf. PAC97, Vancouver, Canada, 1997.

[72] M. Campanelli (private communication).

[73] L. Barret *et al.*, Report No. NuMI-L-551, 1999.

[74] N. Holtkamp (private communication).

[75] K. Dick, M. Freund, P. Huber, and M. Lindner, Nucl. Phys. **B588**, 101 (2000).

[76] CNGS conceptual design report No. CERN 98-02.

[77] Talk presented by A. Riche at the Joint U.S./Japan Workshop on New Initiatives in Muon Lepton Flavor Violation and Neutrino Oscillation with High Intense Muon and Neutrino Sources, Honolulu, Hawaii, 2000, http://meco.ps.uci.edu/lepton_workshop/talks/riche.pdf

[78] V. Barger, S. Geer, R. Raja, and K. Whisnant (in preparation).

[79] N. Gehrels, Astrophys. J. **303**, 336 (1986).